IEEE Access
Multidisciplinary | Rapid Review | Open Access Journal

Received May 17, 2021, accepted June 6, 2021, date of publication June 16, 2021, date of current version June 30, 2021.

Digital Object Identifier 10.1109/ACCESS.2021.3089762

The IEEE-SA Working Group on Spaceborne GNSS-R: Scene Study

HUGO CARRENO-LUENGO[1], (Senior Member, IEEE), ADRIANO CAMPS[2,3], (Fellow, IEEE), CHRIS RUF[1], (Fellow, IEEE), NICOLAS FLOURY[4], MANUEL MARTIN-NEIRA[4], (Senior Member, IEEE), TIANLIN WANG[1], (Member, IEEE), SIRI JODHA KHALSA[5], (Senior Member, IEEE), MARIA PAOLA CLARIZIA[6], (Senior Member, IEEE), JENNIFER REYNOLDS[6], JOEL JOHNSON[7], ANDREW O'BRIEN[7], (Member, IEEE), CARMELA GALDI[8], (Member, IEEE), MAURIZIO DI BISCEGLIE[8], (Member, IEEE), ANDREAS DIELACHER[9], PHILIP JALES[10], MARTIN UNWIN[11], LUCINDA KING[12], (Graduate Student Member, IEEE), GIUSEPPE FOTI[13], RASHMI SHAH[14], (Senior Member, IEEE), DANIEL PASCUAL[6], (Member, IEEE), BILL SCHREINER[15], MILAD ASGARIMEHR[16], JENS WICKERT[16,17], SERNI RIBO[3,18], (Member, IEEE), AND ESTEL CARDELLACH[3,18], (Senior Member, IEEE)

[1]Climate and Space Sciences and Engineering Department, University of Michigan (UM), Ann Arbor, MI 48109, USA
[2]CommSensLab-UPC, Universitat Politecnica de Catalunya (UPC), 08034 Barcelona, Spain
[3]Instiut d'Estudis Espacials de Catalunya (IEEC), 08034 Barcelona, Spain
[4]European Space Research and Technology Center (ESTEC), European Space Agency (ESA), 2201 Noordwijk, The Netherlands
[5]National Snow and Ice Data Center (NSIDC), University of Colorado, Boulder, CO 80309, USA
[6]Deimos Space UK, Didcot OX11 0QR, U.K.
[7]Electrical and Computer Engineering, The Ohio State University, Columbus, OH 43210, USA
[8]Dipartimento di Ingegneria, Universita degli Studi del Sannio, 82100 Benevento, Italy
[9]RUAG Space GmbH, 1120 Vienna, Austria
[10]Spire Global, Boulder, CO 80301, USA
[11]Surrey Satellite Technology Ltd. (SSTL), Guildford GU2 7YE, U.K.
[12]Surrey Space Centre, University of Surrey, Guildford GU2 7XH, U.K.
[13]National Oceanography Center (NOC), Southampton SO14 3ZH, U.K.
[14]Jet Propulsion Laboratory (JPL), California Institute of Technology, Pasadena, CA 91109, USA
[15]University Corporation for Atmospheric Research (UCAR), Boulder, CO 80305, USA
[16]German Research Centre for Geosciences (GFZ), 14473 Potsdam, Germany
[17]Institute of Geodesy and Geoinformation Science, Technische Universität Berlin, 10623 Berlin, Germany
[18]Institute of Space Sciences (ICE), 08193 Barcelona, Spain

Corresponding author: Hugo Carreno-Luengo (carreno@umich.edu)

This work was supported in part by the National Aeronautics and Space Administration (NASA) Science Mission Directorate with the University of Michigan under Contract NNL13AQ00C.

ABSTRACT The Institute of Electrical and Electronics Engineers (IEEE) Geoscience and Remote Sensing Society (GRSS) created the GRSS "Standards for Earth Observation Technical Committee" to advance the usability of remote sensing products by experts from academia, industry, and government through the creation and promotion of standards and best practices. In February 2019, a Project Authorization Request was approved by the IEEE Standards Association (IEEE-SA) with the title "Standard for Spaceborne Global Navigation Satellite Systems Reflectometry (GNSS-R) Data and Metadata Content." At present, 4 GNSS constellations cover the Earth with their navigation signals: The United States of America (USA) Global Positioning System GPS with 31 Medium Earth Orbit (MEO) operational satellites, the Russian GLObal'naya NAvigatsionnaya Sputnikovaya Sistema GLONASS with 24 MEO operational satellites, the European Galileo with 24 MEO operational satellites, and the Chinese BeiDou-3 with 3 Inclined GeoSynchronous Orbit (IGSO), 24 MEO, and 2 Geosynchronous Equatorial Orbit (GEO) operational satellites. Additionally, several regional navigation constellations increase the number of available signals for remote sensing purposes: the Japanese Quasi-Zenith Satellite System QZSS with 1 GSO and 3 Tundra-type orbit operational satellites, and the Indian Regional Navigation Satellite System IRNSS with 3 GEO and

The associate editor coordinating the review of this manuscript and approving it for publication was Kegen Yu.

4 IGSO operational satellites. On the other hand, there are different GNSS-R processing techniques, instruments and spaceborne missions, and a wide variety of retrieval algorithms have been used. The heterogeneous nature of these signals of opportunity as well as the numerous working methodologies justify the need of a standard to further advance in the development of GNSS-R towards an operational Earth Observation technique. In particular, the scope of this working group is to develop a standard for data and metadata content arising from past, present, and future spaceborne missions such as the United Kingdom (UK) TechDemoSat-1 TDS-1, and the National Aeronautics and Space Administration (NASA) CYclone Global Navigation Satellite System CYGNSS constellation coordinated by the University of Michigan (UM). In this article we describe the scene study, including fundamental aspects, scientific applications, and historical milestones. The spaceborne standard is under development and it will be published in IEEE-SA.

INDEX TERMS GNSS-R, IEEE standards association, satellite missions, Earth remote sensing.

I. OVERVIEW OF THE IEEE STANDARD FOR SPACEBORNE GNSS-REFLECTOMETRY

A. INTRODUCTION TO THE STANDARD: STRUCTURE AND CONTENTS

This working group has been assembled to develop this standard with the purpose of unifying and documenting GNSS-R measurements, calibration procedures, and product level definitions (https://standards.ieee.org/). It includes members, collaborators, and contributors from academia, international space agencies, and private industry. In a face-to-face meeting held on November 2019 during the 6th Workshop on Advanced RF Sensors and Remote Sensing Instruments (ARSI'19) and 4th Ka-band Earth Observation Radar Missions Workshop (KEO'19) joint meeting, the need was recognized to develop a standard with a wide range of operations, providing procedure guidelines independently of constraints imposed by current limitations on geophysical parameters retrieval algorithms. As such, this effort aims to establish the fundamentals of a potential virtual network of satellites providing inter-comparable data to the scientific community (Figs. 1,2).

The proposed IEEE standard [1] presented hereafter has been submitted under the sponsorship of GRSS and is limited to GNSS-R [2]–[5]. The IEEE standard was first presented in the 2020 IEEE International Geoscience and Remote Sensing Symposium (IGARSS). Here it is summarized, and it is used as the base of this paper. The primary objectives of the standard are three-fold:

a) To define a comprehensive, accurate, and clear set of low-level parameters that forms a standard product. The choice of parameters shall be sufficient to enable the accurate retrieval of at least the most common GNSS-R products: Ocean wind speed and surface altimetry, Soil Moisture Content (SMC), Above-Ground Biomass (AGB), inland water, and sea ice.

b) To define the procedures that shall be followed to generate the required fundamental and derived observables that configure this standard: Estimation of the nominal specular point, absolute power calibration, correction for path and atmospheric delays in phase, impact of the coherent scattering term in the bistatic radar cross section, estimation of the scattering area, computation of the noise floor, and Radio Frequency Interference (RFI) detection and mitigation.

c) To generate a list of metadata and quality flags that provide as much information as possible to the final users.

B. THE MOST GENERIC GNSS-R OBSERVABLE: THE DELAY DOPPLER MAP

The basic GNSS-R observables are the so-called delay-waveforms and Delay Doppler Maps (DDMs) (Fig. 3). Some GNSS reflectometers provide only power waveforms. Some others are able to deliver their in-phase I and quadrature Q components, and thus providing phase information of the reflected electromagnetic field. The most widely used GNSS-R observable is the power DDM. Power DDMs $\left\langle |Y_r(\tau, f)|^2 \right\rangle$ can be modelled using geometrical and scattering related parameters as follows [4]:

$$\left\langle |Y_r(\tau, f)|^2 \right\rangle = \frac{T_c^2 P_T \lambda^2}{(4\pi)^3} \times \iint \frac{G_T G_R |\chi(\tau - (R_T + R_R)/c, f - f_c)|^2 \sigma^0}{R_T^2 R_R^2} d^2 \bar{\rho}, \quad (1)$$

where T_c is the coherent integration time, P_T is the power of the transmitted signals, λ is the wavelength of the signals, G_T and G_R are the transmitting and receiving antenna gains towards the direction of the reflected radio-link, R_T and R_R are the ranges from the transmitter and the receiver to the specular point, respectively, χ is the Woodward Ambiguity Function (WAF), τ is the delay of the signal from the transmitter to the receiver, f is the Doppler shift of the reflected signal, f_c is aimed to compensate the Doppler shift of the signal, σ^0 is the bistatic scattering coefficient, and $\bar{\rho}$ is the positioning vector of the scattering point on the reflecting area.

The bistatic scattering coefficient can be defined as follows [6]–[9]:

$$\sigma^0 = \sigma^{\text{coh},0} + \sigma^{\text{incoh},0}, \quad (2)$$

FIGURE 1. Artist's view of the UK-TDS-1 satellite. Image credits Surrey Satellite Technology Ltd. (SSTL).

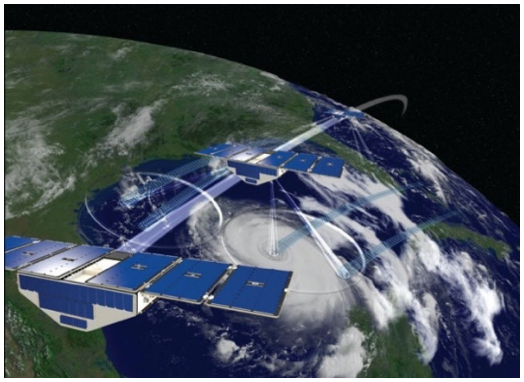

FIGURE 2. Artist's view of the NASA's CYGNSS constellation coordinated by the University of Michigan (UM). Image credits NASA.

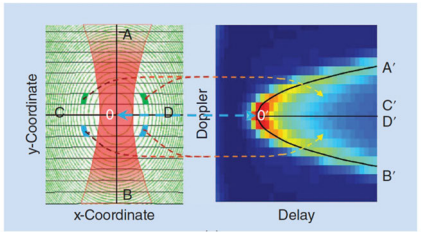

FIGURE 3. Sketch of a sample Delay-Doppler Map (DDM) [4].

where $\sigma^{\text{coh},0}$ and $\sigma^{\text{incoh},0}$ are the coherent and the incoherent scattering terms respectively. Consequently, DDMs consist of a sum of two terms as follows [6]–[9]:

$$\left\langle \left|Y_r(\tau, f)\right|^2 \right\rangle = \left\langle \left|Y_{r,\text{coh}}(\tau, f)\right|^2 \right\rangle + \left\langle \left|Y_{r,\text{incoh}}(\tau, f)\right|^2 \right\rangle. \quad (3)$$

$\left\langle \left|Y_{r,\text{coh}}(\tau, f)\right|^2 \right\rangle$ accounts for coherent reflections from the surface, while $\left\langle \left|Y_{r,\text{incoh}}(\tau, f)\right|^2 \right\rangle$ is responsible for the diffuse scattering.

$\left\langle \left|Y_{r,\text{coh}}(\tau, f)\right|^2 \right\rangle$ can be expressed analytically for the case of an infinite and homogeneously reflecting surface as follows [6]–[9]:

$$\left\langle \left|Y_{r,\text{coh}}(\tau, f)\right|^2 \right\rangle = \frac{T_c^2 P_T \lambda^2 G_T G_R |\chi(\tau, f)|^2}{(4\pi)^2 (R_T + R_R)^2} \times |R(\theta_i)|^2 \gamma \exp(-(2k\sigma \cos\theta_i)^2), \quad (4)$$

where R is the Fresnel reflection coefficient, k is the signal angular wavenumber, σ is the surface height standard deviation (related to small-scale surface roughness), γ is the transmissivity of the vegetation, and θ_i is the incidence angle. $\left\langle \left|Y_{r,\text{incoh}}(\tau, f)\right|^2 \right\rangle$ includes contributions from vegetation, small-scale surface roughness, and topography. Further details on the incoherent scattering over rough surfaces can be found in [4]. The impact of attenuation and scattering by the upwelling vegetation should be considered to establish an accurate model of the incoherently scattered field.

More recently, a new model capable of evaluating both the incoherent and the coherent scattering terms [10] has been developed based on aperture diffraction theory. It has been validated over a lake with spaceborne data as generated using the CYGNSS raw Intermediate Frequency (IF) processor. This model is helpful for accurate analysis of composite scattering from smaller smooth regions interspersed in larger rough terrain.

C. DATA PRODUCTS

An outline of the data products is provided here. Different techniques with a spaceborne application are considered including conventional c-, interferometric i-, reconstructed r-, and partial interferometric pi- GNSS-R. All the complete definitions and details are part of the "Standard for Spaceborne Global Navigation Satellite System-Reflectometry (GNSS-R) Data and Metadata Content" [11].

1) FUNDAMENTAL OBSERVABLES

The following fundamental observables are required to be in agreement with the standard:

- ddm_complex: This field includes the after-correlation in-phase I (real part) and quadrature Q (imaginary part) components of the scattered signal in raw counts. GNSS-R sensors of the c- and r-type shall ideally provide two ddm_complex observables, one for the direct and one for the reflected signal. The GNSS-R sensors of the i-type only need to produce one ddm_complex measurement. The nominal specular point location may be accurately and efficiently computed using e.g. the DTU 10 model over ocean and e.g. the MERIT or Earth 2014 Digital Elevation Model (DEM) over land (or a "reduced" version of these models). Over land, several specular reflection points may be encountered. The number will depend on facet size, but on surface roughness as well, as it widens the angular pattern of the scattered signal [4]. If it is too rough, the pattern will be too wide, and it will not be coherent anymore. These considerations lead to the fundamental question of how to define the specular point: minimum delay?, incidence angle of the incident wave equals incidence angle of the reflected wave? The array size shall be sufficiently large to account for the complete spreading of the DDMs in delay and Doppler domains. State-of-the-art values are ∼4 GPS Coarse Acquisition (C/A)

chips x 5000 Hz or ∼30 GPS C/A chips x 10000 Hz for the C/A code systems. The optimum delay and Doppler bins size are also being analyzed. The bin size shall be defined considering the scientific requirements versus the peak uncertainty. Coherent integration time shall be assumed to be a variable. All information defining the processing approach shall be included as metadata. It is recommended to study the possibility of using direct and reflected signals synchronized in the same correlation channel for system autocalibration.

- ddm_complex_compressed: This is the compressed ddm_complex, i.e. the ddm_complex variable compressed to reduce the number of bits required in its representation. The selected compression approach and any uncertainties introduced shall be included in metadata.
- ddm_complex_cal: This is the calibrated ddm_complex after the application of any corrections for calibration purposes. The calibration method shall be included in the metadata.
- ddm_complex_compressed_cal: This is the calibrated ddm_complex_compressed, after the application of any corrections for calibration purposes. The calibration method shall be included in the metadata.
- ddm_power: This is the uncalibrated power value in raw counts, that is, the squared modulus of ddm_complex or ddm_complex_compressed. The incoherent integration time shall be assumed to be a variable. Default-values for land and ocean surfaces shall be specified for each type of surface. These values shall be included in the nominal operational mode of the receiver. The location of the specular point corresponding to the ddm_power shall be identified. This information shall be included as metadata. ddm_power observables may be produced on-board but also on-ground.
- ddm_power_cal: This is the calibrated power that would have been measured by an ideal GNSS-R sensor. An ideal GNSS-R sensor is one with isotropic antennas and known instrumental gain, delays and offsets, having no quantization errors. Calibration procedures both in delay and amplitude shall be defined including those for cGNSS-R, iGNSS-R, rGNSS-R, and piGNSS-R. Different options exist for calibration. Direct and reflected signals may be routed to a calibration switch circuit inserted between them and their Low Noise Amplifiers (LNAs) which allows for accurate delay and amplitude calibration. Other calibration approaches are possible, including the injection of Pseudo-Random Noise (PRN) signals or using the same antenna for direct and reflected signal. The calibration method shall be included in the metadata.
- phase: This value is the phase [deg] of the calibrated complex (ddm_complex_cal or ddm_complex_compressed_cal) DDMs. The point of the DDMs to what this value corresponds shall be included in metadata. It can be the peak (totally coherent scattering) or the point of maximum derivative of the leading edge of the delay-waveforms (coherent and incoherent scattering terms exist). In the case of GNSS-R sensors of the c- and r-type, phase shall include both direct and reflected correlation channels. The phase shall be corrected for path and atmospheric delays. Such correction shall be also included in the metadata. Note: The use of model based open loop tracking (delay, Doppler) allows phase retrieval without a full waveform sampling [12], [13].
- power: This value is the peak power of the calibrated complex (ddm_complex_cal or the ddm_complex_compressed_cal) and calibrated power (ddm_power_cal) DDMs. In the case of GNSS-R sensors of the c- and r-type the power shall include both direct and reflected correlation channels. The power unit shall be [dBm]. Automatic Gain Control (AGC) shall be stable, and it is recommended to remove any AGC influence by using a constant gain channel.

2) DERIVED OBSERVABLES

The following derived observables are required to be in agreement with the standard:

- brcs: This is the bistatic scattering radar cross section [m^2]. The impact of any coherent scattering term shall be separated. This term shall be also considered for the computation of the overall path loses. The level of the reflected signal relative to the direct signal shall be accurately estimated using preferably the direct signals themselves instead of a look-up table. The GNSS satellites antenna radiation pattern in the direction of the up-looking antenna and the specular point may be assumed to be similar or estimated.
- effective_area: This is an estimate of the effective surface scattering area [m^2] that contributes in terms of power to each DDM bin, after accounting for the GNSS signal spreading function. It may be calculated by convolving the GNSS WAF with the surface area that contributes in terms of power to a given DDM bin as determined by its delay and Doppler values and the measurement geometry. The specular point bin location matches the specular point bin location in the brcs. State-of-the art procedures use an ''end-to-end simulator'' such as the CYGNSS or the Passive Advanced Unit/Passive Reflectometry and Interferometry System (PAU/PARIS) simulator. This information shall be included as a look-up table.
- nbrcs: This value is an estimation of the normalized bistatic scattering radar cross section [dB] derived from dividing brcs by effective_area. For wind speed retrieval, a window of delay and Doppler bins centered in the nominal specular point corresponding to the nominal spatial resolution on Earth's surface should be used (typically) ∼25 km × 25 km for systems using the L1 C/A code (3 delay and 5 Doppler bins in CYGNSS). This window size may be assumed to be a variable, and information shall be included as metadata.

- snr: This value is the Signal-to-Noise Ratio (SNR) of the power DDMs, taking the level of noise floor as reference, in [dB]. In the case of GNSS-R sensors of the c- and r-type, snr shall include both direct and reflected correlation channels.
- noise_floor: This value is the noise floor of the complex (ddm_complex or ddm_complex_compressed) and power (ddm_power) DDMs. In the case of GNSS-R sensors of the c- and r-type, noise_floor shall include both direct and reflected correlation channels. The units of the n_floor are arbitrary units. The computation of n_floor shall account for the type of surface i.e. ocean vs. land, including the effect of topography if needed. It shall be computed as the average over the number of bins before beginning of the leading edge, for all Doppler frequencies in the DDM.
- gamma: This value is the reflectivity computed from the calibrated power (ddm_power_cal) DDMs [dB]. The use of an empirical estimation has been evaluated because both the coherent and the incoherent scattering terms contribute to the peak power of the DDMs [4], [9].
- area and vol: This is the area (area) and the volume (vol) of calibrated power (ddm_power_cal) DDMs. In the case of GNSS-R sensors of the c- and r-type, area_vol shall include both direct and reflected correlation channels. Simulation work indicates that the volume and the area of the DDMs are related to the changes in the contribution to the brightness temperature of the ocean induced by the roughness.
- te and le: This value is the trailing & leading edges width of calibrated power (ddm_power_cal) DDMs in [m]. It is defined as the lag difference between a certain power threshold of the reflected power delay waveforms and the corresponding maximum power of the waveforms. In the case of GNSS-R sensors of the c- and r-type the te and le shall include both direct and reflected correlation channels. The power threshold information shall be included as metadata.
- del: This value is the delay between the peak of the direct power delay waveforms and the point of maximum derivative of the reflected power delay waveforms.
- coh_to_incoh: This value is the coherent-to-incoherent scattering ratio [4], [6].
- coh_comp: This is the coherent component of calibrated power (ddm_power_cal) DDMs. ''Coherent DDMs'' can be generated after removing the influence of the incoherent scattering term by the computation of the variance of the coherently integrated DDMs prior to the incoherent averaging.

II. GNSS-R TECHNIQUES

It is understood that there are several different techniques for producing spaceborne GNSS-R measurements, and it is the intention of the working group that the standard will be applicable generally to all of them. The working group has identified, presently, the 4 current or proposed GNSS-R techniques used in spaceborne applications:

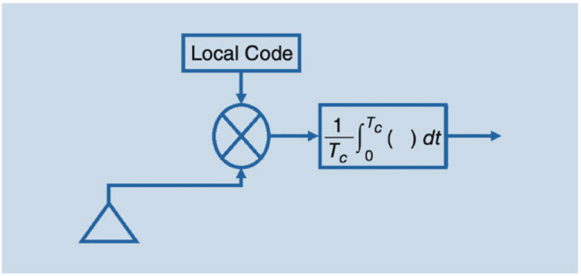

FIGURE 4. Basic concept of a conventional GNSS-R instrument [4].

A. CONVENTIONAL GNSS-R

Conventional GNSS-R (cGNSS-R) (Fig. 4) [5], [14]–[17] correlates coherently during Tc (typically 1 ms for GPS L1 C/A, L5 and Galileo E5; and 4 ms for Galileo E1 OS) the reflected signal with a locally generated replica of the transmitted signal after proper compensation of the Doppler frequency shift, possibly for a number of Doppler frequencies around the central Doppler and/or time delays. cGNSS-R can be used even from platforms with small antennas and relatively low coherent and incoherent integration times. As such, this technique is recommended for land surfaces applications (e.g. soil moisture and biomass monitoring) because of the higher spatial resolution as compared to iGNSS-R (explained in the following) that requires longer integration times because of the lower SNR (unless very large and directive antennas are used).

B. INTERFEROMETRIC GNSS-R

In the interferometric GNSS-R (iGNSS-R) case [5], [14] (Fig. 5) the reflected signal is cross-correlated with a measured direct signal itself after proper Doppler frequency and delay adjustment. iGNSS-R allows exploiting the full spectral density of the GNSS signals (i.e. all the codes are implicitly available, even the encrypted ones), thus improving ranging precision because of the steeper slope of the power waveforms on the tracking point (the point of maximum slope in the leading edge). As such, iGNSS-R can provide enhanced precision in ocean altimetry as compared to cGNSS-R using only the publicly available codes. On the other hand, the SNR [18], [19] is

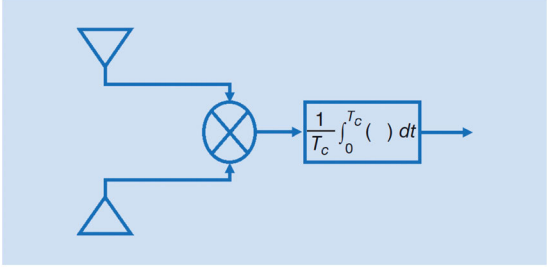

FIGURE 5. Basic concept of an interferometric GNSS-R instrument [4].

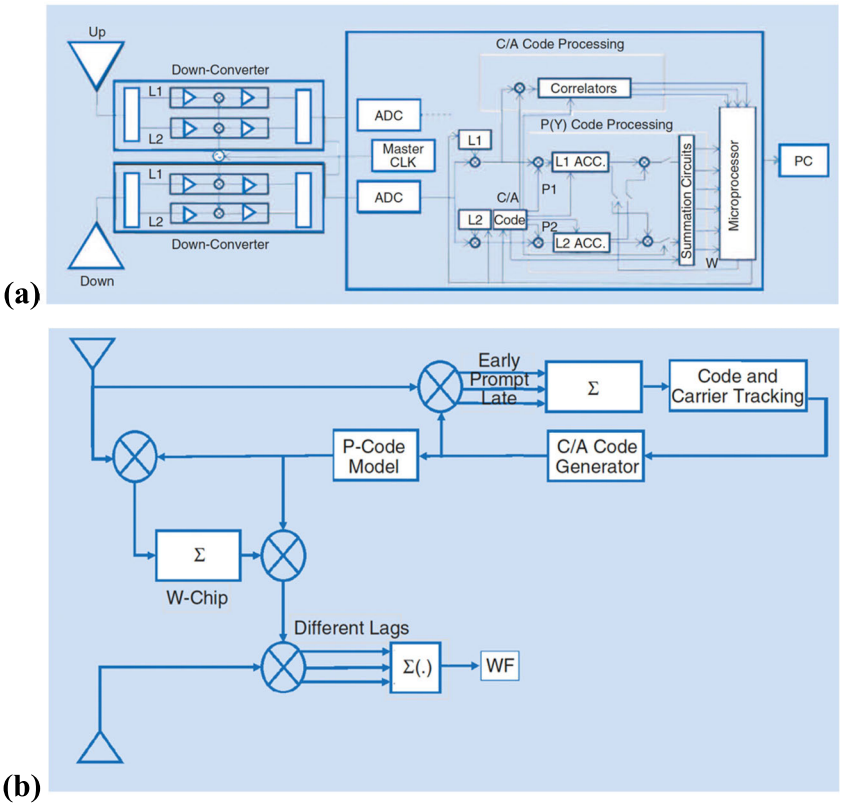

FIGURE 6. **Basic approaches of the reconstructed GNSS-R technique: (a) adapted from [4], [27] and (b) adapted from [4], [28].**

a key-parameter because thermal noise affects both the direct and reflected signal measurements, and the noise of the cross-correlation signal is severely degraded unless the size of the up- and down-looking antennas is increased significantly. Consequently, beam-steering techniques and eventually multi-beam antennas (1 per Space Vehicle SV to be tracked and 1 for its corresponding reflection) are required to guarantee a high spatio-temporal sampling of the surface for mesoscale altimetry. Additionally, a proper calibration process is required to improve the altimetric product accuracy because of instrument thermal and aging drifts. However, a self-calibrated configuration can be used to compensate for these drifts. The Passive Reflectometry and Interferometry System In-orbit Demonstration (PARIS IoD) [14], the GNSS REflectometry, Radio Occultation, and Scatterometry Onboard the International Space Station (GEROS-ISS) [20], and the GNSS Transpolar Earth Reflectometry exploriNg System (G-TERN) [21] Phase A studies, the "Cookie" [22] concept, and several additional works [23]–[25] provide results on the performance of iGNSS-R design. It should be pointed out that this optimization does not apply to a cGNSS-R altimeter, since there is only a down-looking antenna and receiving channel, and any drifts in the frequency response, immediately translate into a delay error that cannot be compensated for.

C. RECONSTRUCTED CODE GNSS-R

Reconstructed-code GNSS-R (rGNSS-R) [27], [28] (Fig. 6) is similar to the cGNSS-R technique, but semi-codeless techniques are used to reconstruct the P(Y) or other codes which are then correlated with the reflected signal. In [27], the correlation approach used in the down-looking channel instrument provides P-code processing of encrypted GPS signals without knowledge of the encrypted code, in addition to the C/A code for cGNSS-R, while the up-looking channels use a similar correlation approach and feed the information to the down-looking channel. In [28], the direct L1 C/A signal is processed with typical Delay Locked Loops (DLLs) and Phase Locked Loops (PLLs). The locked C/A code model is used to form a L1 P model, which is then applied to the direct signal, and after integration over ∼0.5 MHz W-chips to estimate their signs, it is combined with the P-code model to form a L1 Y-code model which is used to correlate with the down-looking channel. The advantages of rGNSS-R rely mainly on the larger bandwidth of the P(Y) codes as compared to the C/A ones, and the larger SNR as compared to iGNSS-R, despite the losses of the semi-codeless approach.

D. PARTIAL INTERFEROMETRIC GNSS-R

Partial interferometric GNSS-R (iGNSS-R) [29] (Fig. 7) is similar to the iGNSS-R technique but using only as reference signal the encrypted large-bandwidth signals (P and M code

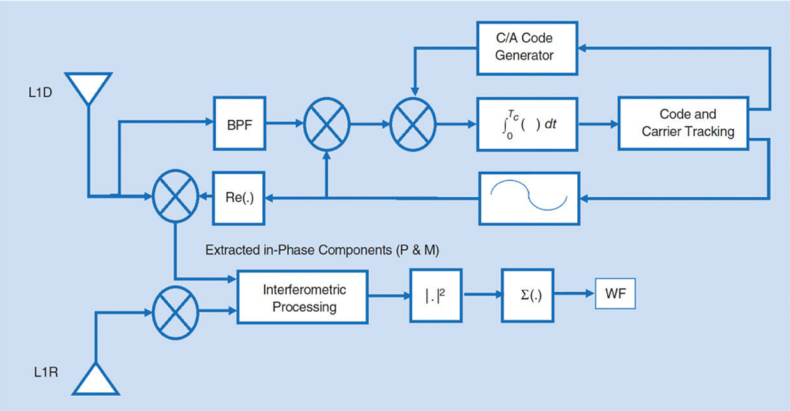

FIGURE 7. Basic approach of the partial interferometric GNSS-R technique (adapted from [4], [29]).

components) of the direct signal. Although the signal bandwidth is the same, the Gabor bandwidth is larger, and so is the achievable range resolution as compared to the iGNSS-R. However, this theoretical improvement comes at the expense of a 3 dB signal loss as the C/A code has been removed, which has to be compensated by a 3 dB larger antenna directivity.

E. COMPARISON OF DIFFERENT TECHNIQUES

At present, cGNSS-R is the most widely used technique. iGNSS-R provides an improved accuracy in ocean altimetry products but requires higher directivity in both the up- and down- looking antennas. On the other hand, instruments of the i-type are much more complex and require a dedicated calibration strategy. However, tracking and re-tracking strategies are of lower complexity because of the lower dynamics as compared to cGNSS-R [30], [31]. In general, the best SNR performance (which could turn into best altimetric performance) is the one given by rGNSS-R. The improvement between the altimetric performance of the iGNSS-R technique with respect to the one achieved by cGNSS-R (C/A code) is at least a factor of 2 [24]. Further studies are required to elucidate the pros and cons of the different techniques for the different scientific applications, including ocean, land, and cryosphere.

III. GNSS-R MISSIONS AND INSTRUMENTS

In defining the GNSS-R standard, a top priority is that it will be applicable to the wide range of past e.g. UK TDS-1 (Fig. 1), present e.g. NASA CYGNSS (Fig. 2), and future spaceborne GNSS-R missions (Table 1), but also to ground-based and airborne instruments (Table 2). In this Section, an overview of the key-parameters of these missions and instruments is provided, including information about the GNSS-R technique, band, polarization, and GNSS system used by the different satellites and instruments.

At present, the most common configuration is [cGNSS-R, L1/LHCP, GPS]. UK TDS-1 [2] and CYGNSS [3] use this configuration, although different signals can also be processed using raw collections of IF samples. BuFeng-1 A/B also follow this configuration, but additionally can collect BeiDou signals [36].

UK TDS-1 (Fig. 1) was launched into space in 2015 with 8 payloads on-board. One of these payloads was a technology demonstrator GNSS-R instrument [33]. UK TDS-1 data were publicly available. As such, the community was able to check and to develop new retrieval algorithms. CYGNSS (Fig. 2) has been the first operational GNSS-R mission launched into space. CYGNSS was first proposed for ocean wind speed estimation over tropical cyclones, although it has been extended to operations over land surfaces. The orbital configuration of each CYGNSS satellites is a circular Low Earth Orbit (LEO) with a height of ∼520 km and an inclination angle of ∼35°. At present, all 8 CYGNSS spacecrafts are healthy and operating nominally [56]. More recently, BuFeng-1 A/B twin satellites were also launched into space. Each platform has 2 Nadir GNSS-R antennas, 1 navigation antenna, 1 auxiliary antenna, 4 LNAs with blackbody calibration, and a GNSS-R receiver. The two Nadir antennas are directed at the left and right sides of the platform with inclination angles of ∼26°. A first feasibility study for wind speed retrieval has been performed [36].

Finally, it is highlighted that ^{3}Cat-2 [34], launched in 2016, was the first CubeSat mission dedicated to GNSS-R. More recently, more CubeSats have also been launched [37], [39].

IV. SCIENTIFIC APPLICATIONS

There are several scientific applications of GNSS-R for different surface types including ocean, land, and cryosphere. This Section provides an overview of the most relevant algorithms, as well as the associated GNSS-R techniques.

A. OCEAN

GNSS Earth-reflected signals can be used as sources of opportunity for mesoscale ocean altimetry and wind speed retrieval with improved spatio-temporal sampling

TABLE 1. GNSS-R spaceborne missions. Left- and Right- Hand Circular Polarization (L, R- HCP).

Mission	Date	GNSS-R type	Band/Pol used	GNSS used
UK-DMC [32]	2003	cGNSS-R	L1 / LHCP	GPS
UK-TDS-1 [33]	2015	cGNSS-R	L1 / LHCP	GPS
CYGNSS [3]	2016	cGNSS-R	L1 / LHCP	GPS
^{3}Cat-2 [34]	2016	cGNSS-R rGNSS-R iGNSS-R	L1, L2 / LHCP, RHCP	GPS GLONASS Galileo BeiDou
SMAP GNSS-R [35]	2017	cGNSS-R	L2 / H, V	GPS
BuFeng-1 A/B [36]	2019	cGNSS-R	L1 / LHCP	GPS BeiDou
Spire series [37]	2019	cGNSS-R	L1 / LHCP	GPS Galileo
Fengyun-3 series [38]	2020	cGNSS-R	L1 / LHCP	GPS Galileo BeiDou
^{3}Cat-5 A/B (FSSCat mission) [39]	2020	cGNSS-R	L1 / LHCP	GPS Galileo
^{3}Cat-4 [40]	2021	cGNSS-R	L1, L2 / LHCP	GPS Galileo
PRETTY [41]	2022	iGNSS-R	L1 / RHCP	GPS Galileo
TRITON [42]	2022	cGNSS-R	L1/LHCP	GPS

as compared to traditional monostatic radar altimetry and scatterometry.

1) OCEAN ALTIMETRY

The potential of c/iGNSS-R for ocean altimetry (Fig. 8) was first published in 1993 [5]. Over smooth ocean surfaces, the altimetric range as it is obtained from the delay of the peak was first proposed in [57]. In 2002, a new approach was formulated which consists in fitting a theoretical model to the data. The best fit model implicitly indicates the delay location where the specular point lies [58]. In 2010, it was demonstrated that the maximum of the derivative of the waveform's leading edge corresponds to the specular ray-path delay (except for filtering effects of the limited bandwidth) [59]. The DDM multi-look technique was proposed later. It consists in the acquisition of the full DDM as a way to perform multi-look altimetry beyond the typical pulse-limited region [60]. Additionally, improved altimetric techniques based on phase observations have been tested from an aircraft [61], [62] and a zeppelin [63]. The results, for low elevation angles up to $\sim 30°$, show altimetric precisions comparable to Nadir-looking peak-derivative methods over open sea waters. These results have been confirmed from space, both in near-Nadir geometry over smooth sea ice surfaces [64] and grazing-angle geometries over sea ice and ice sheets [65] and over relatively calm seas [66]. All of the above algorithms are based on cGNSS-R. The peak-derivate method has also been applied in 2013 to iGNSS-R [24], and in 2014 to rGNSS-R [27].

Finally, it is worth to comment that in the spaceborne era, the peak-derivative method [67], [68], and the phase observations [66] have also been successfully explored using cGNSS-R. An alternative approach similar to the peak-derivative method was proposed in [24]. It consists in assuming that the specular path delay corresponds to the delay at the 75% [24] and 70% [69] of the peak power. In order to achieve the centimetric accuracy required to track the mean sea level and its spatio-temporal variations, related to large-scale circulation, ocean currents and eddies, or El Niño events, one of the challenging errors to be corrected for is the Electro-Magnetic (EM) bias, which in GNSS-R it also exhibits a dependence with the elevation and azimuth angles [70]–[72]. Additionally, bandwidth has an important impact in the iGNSS-R waveforms [73]. As the bandwidth is reduced, the Auto Correlation Function (ACF) becomes wider, and the waveform shape approximates to the cGNSS-R approach, using the C/A code only. The displacement produced is small for 20 MHz (40 MHz in RF) (around 14 cm approx.). At 10 MHz (20 MHz in RF), the displacement obtained is around 25 cm, which could start to be relevant.

TABLE 2. Summary of some available information on some existing GNSS-R receivers. Type of GNSS-R instruments: G (Ground-based), A (Airborne), S (Spaceborne). GPS-IR means GPS interferometric reflectometry, which is a dedicated ground-based technique.

ID	HW/ SW	Number RF Ports	Frequency Bands	BB Bandwidth (MHz)	Sampling Rate (MHz)	Output Rate (Hz)	Receiver Technique	GNSS Constellation	Type
GORS-1(2) [43]	HW	2 (4)	L1, L2	-	-	-	cGNSS-R (C/A, L2C)	GPS, Galileo	G, A
TR	SW	2	L1, L2	-	-	-	Raw	GPS	G
BJ	SW	4	L1, L2	18	20	20,000	Raw	GPS	G
TriG (extended)	HW	8 (16)	Any 4 within L-band	2 to 40 config.	20/40	0.1-1000	Any: software config.	GPS, GLONASS Galileo	G
OceanPal/ SAM	SW	2	L1	4	16.367	1000	Raw	GPS	G
OpenGPS [44]	HW	2	L1	-	5.7	<1000	cGNSS-R (C/A)	GPS	G
COMNAC	SW	1	L1	-	5.7	-	Raw	GPS	G
Ublox LEA-4T	HW	1	L1	2	4	-	cGNSS-R (C/A)	GPS	**G**
NordNav	SW	1(4)	L1	2	16.4	-	Raw	GPS	G
GRAS	HW	3	L1, L2	20	28.25	1000	cGNSS-R (C/A)	GPS	G
DMR [45]	HW	4	L1, L2	4	16	variable	cGNSS-R, raw	GPS	S
NGRx [46]	HW	20	L1, L5	32	65	variable	cGNSS_R, raw	GPS, Galileo, other	S
POLITO-GNSS-R	SW	1	L1	-	8.1838	-	Raw	GPS	G
GRIP-SAR GO	HW	2	L1, L5, E1, E5	52	<=150	1	cGNSS-R	GPS Galileo	G
GLORI [47]	SW	4	L1	4	16.4	-	cGNSS-R	GPS	A
GOLD-RTR [48]	HW	3	L1	8	20	1000	cGNSS-R (C/A)	GPS	G, A
PIR/A [49]	HW	3	L1	12	80	1000	iGNSS-R	Any at L1	G, A
SPIR [50]	SW	16	L1, L5	80	40	40000	Raw	Any at L1, L5	G, A
SPIR--UAV	SW	8	L1, L5	80	40	40000	Raw	Any at L1, L5	A
DODEREC [51,52]	HW	3	L1	-	20.46	-	cGNSS-R (C/A)	GPS	G
SMIGOL [53]	HW	1	L1	2.2	5.745	1	GPS-IR (C/A)	GPS	G
PYCARO [27,54]	SW	2	L1, L2	20	> 100 MHz	Tc and Ti config.	cGNSS-R, rGNSS-R iGNSS-R	GPS, GLONASS, Galileo, BeiDou	G, A, S
PYCARO-2	SW	2	L1, L2, L5 B1, B2, B3 E1, E5	50	> 100 MHz	1	cGNSS-R, rGNSS-R	GPS, GLONASS, Galileo, BeiDou	G
MIR [26]	HW/ SW	2	L1, L5	24	32.736 (x2)	Tc and Ti config.	Raw	GPS Galileo	G, A
FMPL-1 [40]	HW/ SW	2	L1, L2	2	4.096	Tc and Ti config.	cGNSS-R	GPS	S
FMPL-2 [55]	HW/ SW	2	L1, E1	2.4	4.096	Tc = 1 or 4 ms; Ti config	cGNSS-R	GPS L1 C/A Galileo E1	S
FMPL-3	HW/ SW	2	L5 E5a	24	10.230	Tc and Ti config	cGNSS-R	GPS L5 Galileo E5a	S
GENESIS	HW	16	All L-band	-	2 – 40 I/Q config.	1000	cGNSS-R, GNSS-RO, GNSS-PRO	All GNSS and SBAS, >=2 freq. each	A, S

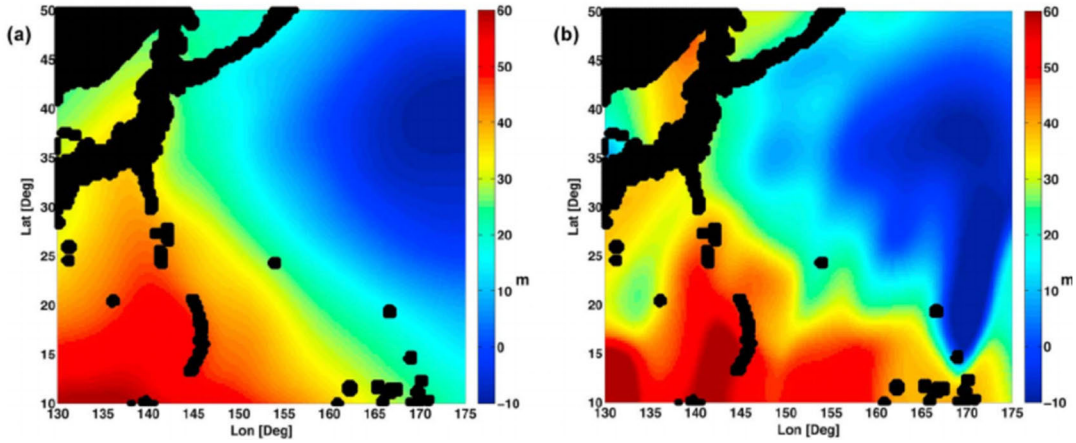

FIGURE 8. (a) Image of [67]: Technical University of Denmark (DTU) 10 Mean Sea Surface Height (MSSH) over the North Pacific, (b) UK TDS-1 derived MSSH.

2) WIND SPEED

The first wind speed retrieval algorithms were based on the so-called DDM-fit method [74]–[76]. After re-normalizing and re-aligning the delay-waveform, the best fit against a theoretical model gives the best estimate for the geophysical and instrumental-correction parameters.

Depending on the model used for the fit, the geophysical parameters can be 10-meter altitude wind speed, or sea surface slopes' variance (Mean Square Slopes MSS). Alternative methods perform the fit on the DDM [77], [78]. In this way, anisotropic information can be obtained from a single satellite observation. In the so-called trailing-edge methods, the fit is performed on the slope of the trailing-edge [75], [79]. Additionally, a stochastic method has been proposed [80]. It consists of two algorithms to relate the sea roughness conditions with the Doppler spread and the delay spread of the reflected signals. This technique was applied to LEO-based GNSS-R data from the UK-DMC mission [81], where five GNSS-R measured Doppler spreads correlated with the MSS records taken by nearby buoys.

In 2008, simulations indicated that the volume under the normalized DDM or the area under the normalized waveform up to a predetermined threshold are due to the changes in the surface roughness, signals which in turn are also captured in the brightness temperature of the ocean L-band emission [82]–[84]. Simultaneously, the discrete-Probability Density Function (PDF) method was also proposed [85]. When the bistatic radar equation for GNSS signals is re-organized in a series of terms, each one depending on the surface's slope, the system is linear with respect to the PDF of the slopes. Discrete values of the PDF are therefore obtained. This retrieval does not require an analytical model for the PDF (no particular statistics assumed). When the technique is applied on DDMs, it is possible to obtain the directional roughness, together with others non-Gaussian features of the PDF (such as up/down-wind separation). In 2011 the Normalized Radar Cross Section (NRCS) inversion method was formulated [86]. Numerically efficient methods were presented [86], [87] for inverting DDMs to produce a 2-D mapping of the NRCS over the glistening zone [86], [87]. All of the above algorithms are based on cGNSS-R.

A feasibility study of wind speed retrieval from space was performed using data from the UK TDS-1 mission [88]. The most successful example of GNSS-R mission for wind speed retrieval is the CYGNSS mission [3], designed primarily for the purpose of monitoring tropical cyclones [89]–[92], but collecting data over all of the oceans and providing global retrievals of wind speeds [93]–[95]. These retrievals are achieved using the so-called baseline approach, that implements the minimum variance combination of wind estimates from two observables derived from CYGNSS DDMs, which are known as Delay Doppler Map Average (DDMA) and Leading-Edge Slope (LES) [93]–[95]. Wind speed estimates derived from each of these observables are obtained via the development of Geophysical Model Functions (GMFs), which consist of 2-D lookup tables of retrieved wind speed, as a function of the observable and the incidence angle (Fig. 9) [95]. The baseline winds provide good quality global wind estimates which have been shown to meet the mission requirements [96], but suffer from significant retrieval biases, especially at high wind speeds [97]. More recently, a retrieval algorithm based on the use of an Artificial Neural Network (ANN) has been also proposed for wind speed estimations from CYGNSS [98].

3) SWELL

At present, there are few studies on the impact of swell on GNSS-R. However, the scattering at L-band can be significantly affected by swell. In 2012, the superposition of the wave spectrum with the swell was evaluated in [99]. In 2013, an air-borne experiment suggested the possibility to measure sea waves periods and heights [100]. That evidence triggered the need to better understand the scattering mechanisms, and to that end, an experiment was performed over a wave channel, showing the feasibility to perform sea waves

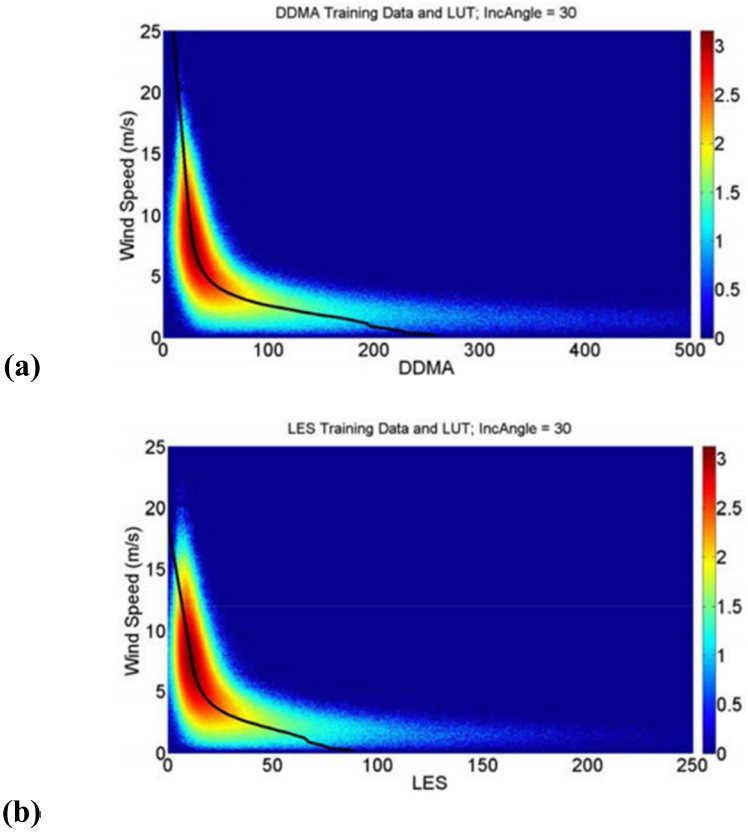

FIGURE 9. Empirical Geophysical Model Functions (GMFs) for the two Level 1 observables: (a) Delay Doppler Map Average DDMA, and (b) Leading Edge Slope LES, at an incidence angle of ∼30°, overlaid on log (density) scatter plots of the training data from which they were derived [95].

determination using coherently reflected GPS signals [101]. Simultaneously, the effects of swell on the EM bias were evaluated as a function of the elevation angle [72]. In 2016, the existence of swell effects in low wind speed conditions were analyzed with UK TDS-1 data [102]. In 2020, an analysis in three domains (statistical, time, and spectrum) using airborne data [103], [104] showed the possibility to retrieve wind-driven waves period and swell period thanks to the identification of the secondary peaks [6] present on the coherent component, and other derived products such as the sea state, and the sea surface height with improved resolution. Finally, simulation studies with effects of swell have been compared with TDS-1 data, showing that swell changes the sea surface roughness and has a significant impact on the scattering of GNSS-R signals [105].

4) TARGET DETECTION

GNSS-R constellations could revolutionize sea target detection thanks to the improved spatio-temporal sampling properties [106]–[110]. In [106], airborne experimental data demonstrated the possibility of ship detection. In [107], the use of DDMs acquired in a backscattered configuration was proposed. The feasibility of sea target detection from a spaceborne platform was showed in [108] using a spatial filter based on steerable antenna beams to solve for the mapping ambiguity. [109] presented a Constant False Alarm Rate (CFAR) method for ship object detection. In [110], a sea target detection algorithm with a spaceborne application was described. It was based on a sea clutter compensation step, using an adaptive threshold to consider spatial variability in the sea background and/or noise statistics. More recently, a few more works [111], [112] have provided new insights. In [111], a matched filter was proposed using data from the UK-TDS-1 to detect sea-targets in a DDM sequence without requirements for any (pre)detection. Finally, simulations for ship detection applications at low incidence angle were performed in [112] using a stochastic simulator for sea surfaces.

B. LAND

The use of different GNSS-R techniques for land-surface applications requires further research activities because the dielectric properties of this scattering medium make it more complex than the ocean surface.

1) SOIL MOISTURE CONTENT

The first study on the potential use of GNSS-R for SMC estimation was published in 2000 [113]. Follow-on activities were proposed simultaneously to investigate the

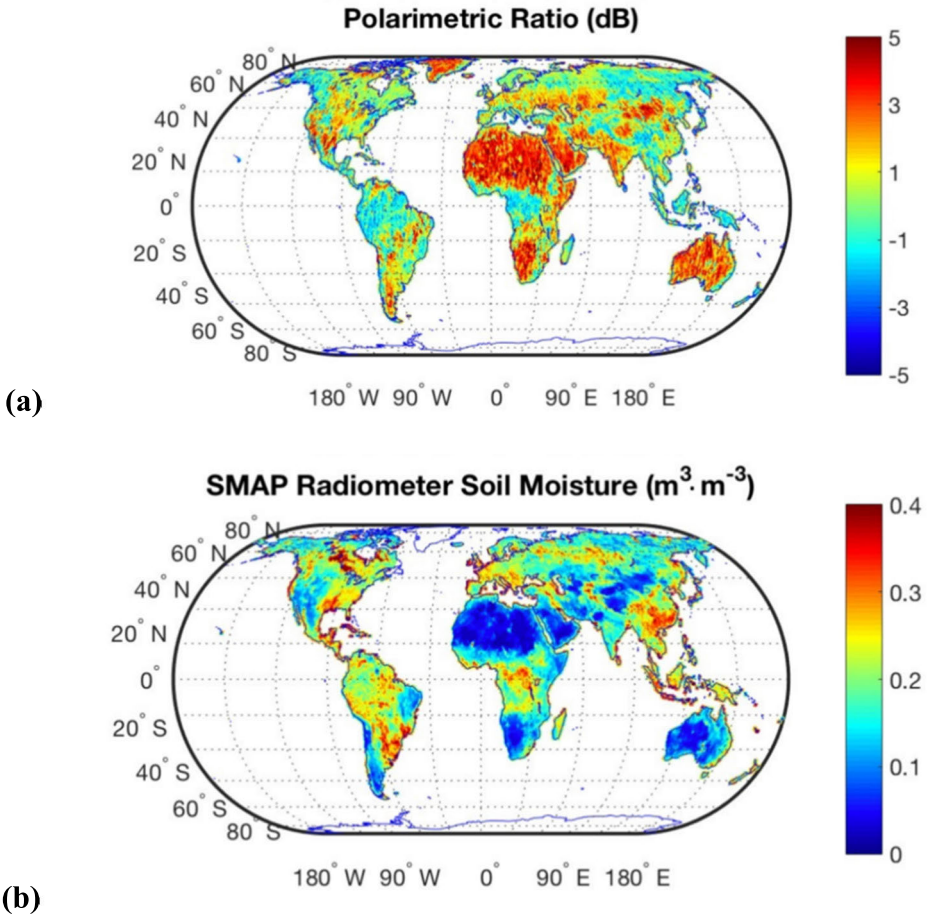

FIGURE 10. SMAP over-land power waveform analysis using one-year averaged values [35]: (a) Polarimetric ratio, (b) global distribution of time-averaged retrieved surface soil moisture based on SMAP radiometer observations and application of the multi-temporal dual-channel algorithm [125].

capabilities of GNSS-R for SMC determination using cGNSS-R [114]–[116] and GPS Interferometric Reflectometry (GPS-IR) [53], [117]–[119]. The use of the polarimetric ratio (ratio of the reflected signals' power at two different polarizations) on cGNSS-R data collected from two airborne experiments was further studied for SMC determination because it can cancel out surface roughness effects [35], [120]. A GNSS dual-polarization payload [27] was successfully tested during two experiments from a stratospheric balloon [6]. A comprehensive study over different land surface types was performed to further assess the use of dual-polarization information obtained during two air-borne campaigns [121].

More recently, new important conclusions were also derived. The use of the GPS-IR for accurate SMC estimation was validated over multiple GPS test sites including vegetated surfaces [118], [122]. A sensitivity to SMC of $\sim$38 dB/(m^3/m^3) was measured over nearly bare-soil target areas using data from UK TDS-1 [123], [124]. A Pearson correlation coefficient of r $\sim$ -0.6 between 1 year averaged polarimetric ratio from a GNSS-R experiment onboard the Soil Moisture Active Passive (SMAP) mission and SMC (Fig.10) was measured over the complete Earth's surface [35], [125]. The elevation angle should be considered for the application of the so-called Tau-Omega model in the GNSS-R case [9]. Daily averaged CYGNSS-derived and SMAP-derived SMC showed a good agreement over specific test sites [126]. A better sensitivity of CYGNSS to SMC appeared over croplands when the coherent scattering term became dominant over the incoherent one, with a sensitivity to SMC of $\sim$50 dB/(m^3/m^3) [127]. It was found that the ratio of the coherent-to-incoherent scattering terms depends on the elevation angle [127], [128]. The reflectivity was found to be a better SMC estimator than the SNR. Additionally, it was found a significant influence of the elevation angles on the results [128].

Several works have demonstrated the possibility to estimate SMC using CYGNSS data. A retrieval approach based on incoherent scattering was presented in [129], under the assumption that vegetation and roughness changes occur on timescales longer than those associated with soil moisture changes. Results suggested that global SMC retrieval with an RMS error on the order of $\sim$0.04 cm^3/cm^3 is possible over varied terrain (Fig. 11). Simultaneously, the

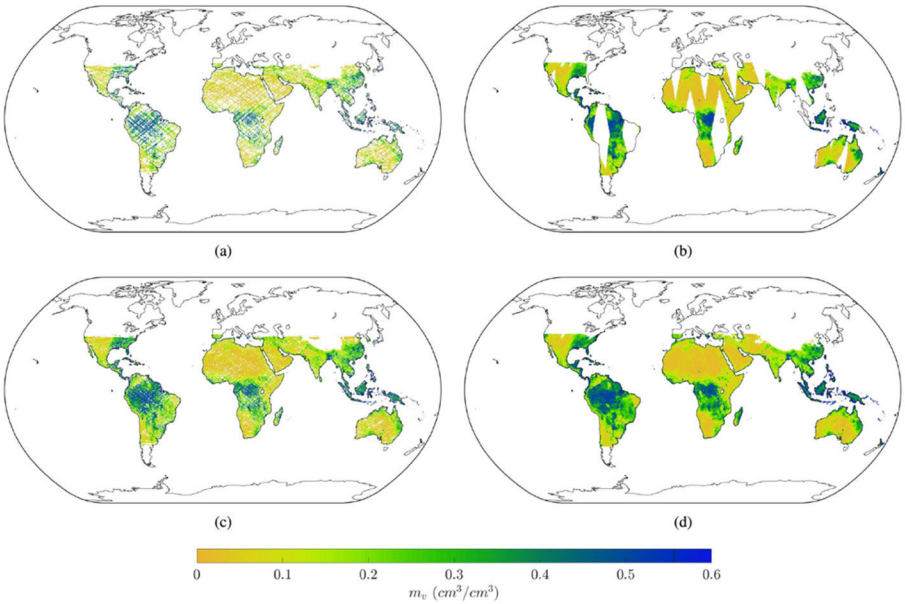

FIGURE 11. Comparisons of SMAP and CYGNSS SMC [129] on time scales of 1 day and 3 days on a 0.2° × 0.2° latitude/longitude grid. (a) Retrieved SMC using CYGNSS land returns over 1 day, (b) SMAP SMC over 1 day, (c) retrieved SMC using CYGNSS land returns over 3 days, (d) SMAP SMC over 3 days.

so-called Reflectivity-Vegetation-Roughness R-V-R algorithm was implemented in [130]. The CYGNSS-derived SMC values that were estimated globally agreed well with SMAP collocated measurements, delivering an overall RMS error of ∼0.07 cm^3/cm^3. The University Corporation for Atmospheric Research (UCAR) / University of Colorado (CU) SMC product was presented in [131]. This product was derived using the empirical relationships between the reflectivity and SMAP-derived SMC. It was validated at 171 in-situ soil moisture stations, which resulted in a median unbiased RMSE of ∼0.049 cm^3/cm^3. At present, the main remaining challenges are to properly correct for the impact of the upwelling vegetation cover and the small-scale surface roughness in the reflectivity, so as to improve the accuracy in SMC retrievals [132]. To do so, multi-pass and single-pass techniques can be applied, each one with pros and cons. Finally, it worth to mention that a significant effort has been performed in the development of simulation tools to better understand SMC retrieval capabilities from a space-borne platform [133].

2) BIOMASS

Some pioneering studies showed a promising sensitivity to forest biomass. Scattering simulations based on the Bistatic MIchigan MIcrowave Canopy Scattering (Bi-MIMICS) model at linear polarization (Horizontal H, Vertical V) suggested a better sensitivity than monostatic configurations for canopy Height CH ∼8 m [134]. This result was consolidated using the Tor Vergata model at circular polarization (RHCP, LHCP) for higher levels of biomass up to AGB ∼200 ton/ha [135]. Direct and multiple scattering terms were evaluated using Bi-MIMICS [136] at circular polarization (RHCP, LHCP). It was concluded that the total scattering field at both polarizations RHCP and LHCP is dominated by the scattering over the tree trunks layer. The Soil and Vegetation Reflection Simulator (SAVERS) was developed using the Tor Vergata electromagnetic model [135]. SAVERS includes capabilities to predict signal power as measured by a GNSS-R reflectometer, considering system properties, and observation geometry [116]. Two airborne experiments confirmed the sensitivity of the bistatic reflectivity up to high levels of AGB ∼300 ton/ha [137].

Empirical results over boreal forests from a stratospheric balloon suggested that the coherent scattering term is roughly independent of the platform's height [138]. The EMISVEG [139] and the Signals of opportunity Coherent Bistatic scattering model for Vegetated terrains (SCoBi-Veg) [140] simulators further analyzed this hypothesis. Lindenmayer systems [141] were used to generate fractal geometry and the Foldy's approximation [142] was used to account for attenuation and phase change of the coherent wave propagating in the forest media. More recently, a comprehensive study [143] demonstrated a significant sensitivity of several GNSS-R observables up to AGB ∼150 ton/ha at different elevation angles using the GLObal navigation satellite system Reflectometry Instrument (GLORI) instrument [47]. Feasibility studies for the case of GNSS-R data collected from a spaceborne platform have shown a certain sensitivity to forests biomass on a global scale using the SMAP radar receiver [35]. CH was demonstrated to be a key parameter, with a higher impact in GNSS-R signatures than Normalized Difference Vegetation Index (NDVI). More

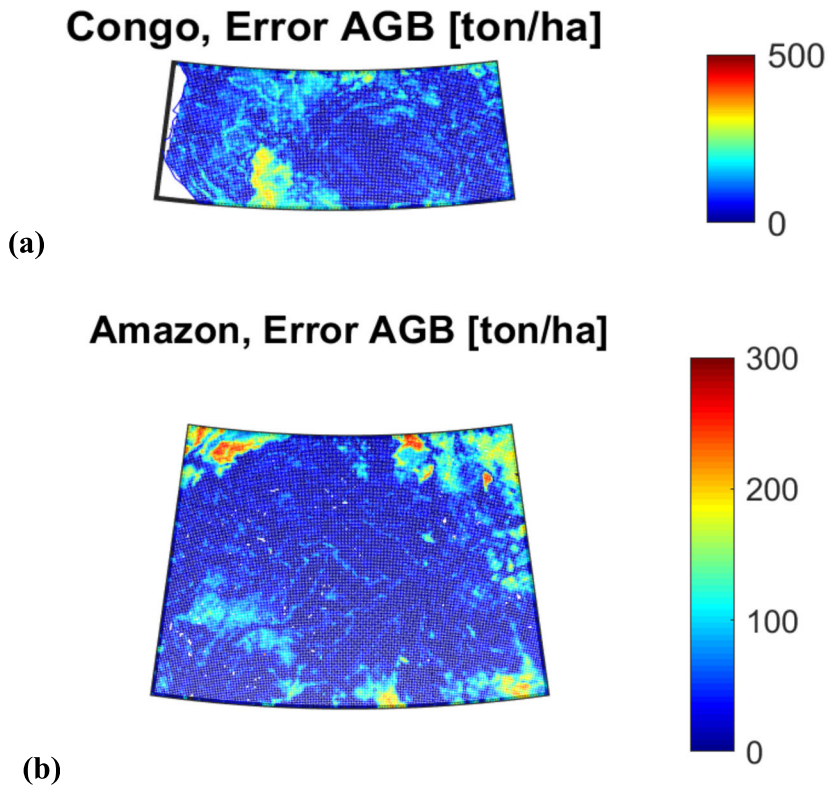

FIGURE 12. Absolute error in AGB retrieval over (a) Congo, and (b) Amazon [144]. Trailing edge was used at grazing angles. Empirically derived polynomial fitting functions were used.

recently, the first maps of absolute error in AGB retrieval from space using GNSS-R were generated, showing a small error over areas with an AGB up to ∼500 ton/ha (Fig. 12). These findings suggest the possibility of accurate AGB retrieval using GNSS-R on-board small satellites such as, e.g., CYGNSS [144]. Additionally, experimental results have suggested that for beech forest, NDVI is a good descriptor of signal attenuation at L-band, which is known to be related to the Vegetation Optical Depth (VOD) [145]. Depolarization effects were also studied and they were found to be significant at elevation angles as large as ∼50° [145].

3) INLAND WATER BODIES

GNSS-R data have also been exploited for inland water monitoring thanks to the enhanced spatial resolution and increased reflected power under the coherent scattering regime [146]–[149]. GNSS-R airborne data collected over the Ebro River Delta (Spain) and spaceborne data over the Mississippi River (USA) demonstrated that inundated wetlands can be identified under different vegetation conditions [146]. Later, [147] showed that CYGNSS data provide clear evidence of surface saturation and inundation extent over land with higher spatio-temporal sampling than more traditional microwave radiometers such as e.g. SMAP. [148] showed that CYGNSS watermasks provide accurate, time-varying maps that are able to resolve changes in lake and river position and extent. [149] demonstrated that CYGNSS has a capability for frequent, high-resolution observations of wetland dynamics across a wide range of timescales in the tropics. Finally, [150] demonstrated the creation of dynamic inland water body masks at spatial resolutions ranging from 1 to 3 km through the use of a recently developed coherence detector for the delay-Doppler maps produced by the CYGNSS constellation.

C. CRYOSPHERE

At present, there is also an increasing number of GNSS-R applications in the cryosphere.

1) SNOW

The first study on GNSS-R over thick dry snow masses was the theoretical investigation performed in [151]. Later, the GPS-IR technique was used in several experiments, including the use of frequency [152], and frequency and amplitude [153] measurements. In 2011, the use of the GPS-IR at linear [154] and circular [155] polarization was explored. Alternatively, radio-holographic techniques were used on each lag of the delay-waveform to identify the spectral content of the signal, and to identify each frequency-component to different snow depths, reaching

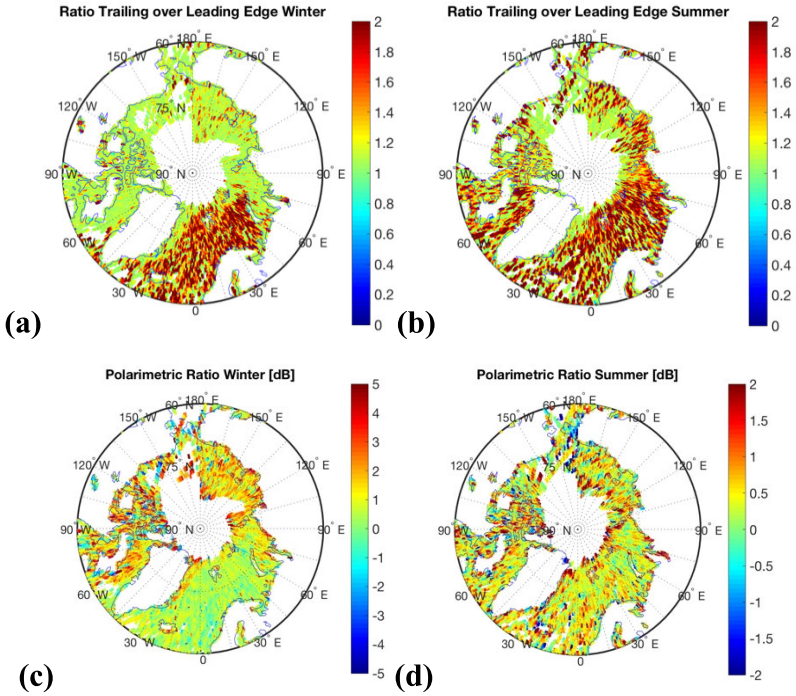

FIGURE 13. Ratio of the trailing over the leading edge [164]: (a) Winter, (b) Summer. Polarimetric Ratio [164]: (c) Winter, (d) Summer.

down to ∼300 meters depth in polar ice sheets of the Antarctica [156].

2) SEA ICE

In 2011, phase-delay observations [155]–[157] were used to monitor the tidal signatures of floating sea ice in Greenland. Alternatively, the peak-power method was used to estimate the permittivity [158]. An empirical model was generated after comparison of the peak power of GPS reflections received by air-borne instruments with RADARSAT backscattered peak power. This method was also applied to spaceborne UK-DMC data and compared to Sea Ice Concentration (SIC) measurements obtained with the Advanced Microwave Scanning Radiometer-E (AMSR-E) and ice charts [159]. However, this observable can be strongly affected by the sea ice surface roughness. To overcome this limitation, the polarimetric ratio was explored in [160]. Linear [161] and circular [162] polarimetric phase shift methodologies were used as a means to estimate the permittivity. A different approach to obtain the sea ice roughness by fitting the waveform shape was used in [162], [163]. This method showed potential for characterization of the different stages of sea ice after the comparison with other remote sensing techniques. In 2013, the scatterometric fit method [156] was used to estimate sea ice roughness. In 2011, a certain correlation was found [155], [156] between the coherence time of the reflected signals and the wind over the zone. All of the above algorithms are based on cGNSS-R.

In the spaceborne era, a GNSS-R study was performed over the Artic from SMAP in 2017 [35], [164], [165]. The sensitivity of several observables (SNR, polarimetric ratio, ratio of the trailing- over the leading- edge, and slope of the trailing-edge) to seasonal fluctuations of SIC was evaluated. The use of the polarimetric ratio at linear polarization was found to provide improved results (Figs. 13,14). This observable followed the Fresnel reflection coefficients for a smooth surface (sea ice): >2 dB (Winter) vs. ∼0.5 dB (Summer). Additionally, several spaceborne experiments have been performed from the UK TDS-1. In 2017, a sea ice detection algorithm was developed using data over the Arctic and the Antarctic regions based on the similarity of the received GNSS reflected waveform to the coherent reflection model waveform [166].

In 2018, the use of Convolutional Neural Networks (CNNs) was proposed for sea ice detection and SIC prediction [167]. In 2019, a framework that employs Support Vector Machines (SVMs) was proposed for the classification of DDMs, specifically, for separating DDMs of sea ice from those of sea water [168]. The developed approach shows improved sea ice detection performance with respect to the existing NN- and CNN-based algorithms in terms of, first, enhanced accuracy and improved robustness with respect to false alarm, second, less DDM data storage requirements, and finally, fewer tuning parameters [169]. In 2020, an effective schematic was developed for estimating Sea Ice Thickness (SIT) from the reflectivity, which was formulated as the product of the propagation loss due to SIT and the reflection coefficient of underlying sea water [170]. A GMF for SIC retrieval has been also developed based on a new observable termed as differential delay waveform (DDW) [171]. Finally, the potential of GNSS-R to classify ice types during the sea ice formation period was demonstrated using a sea ice

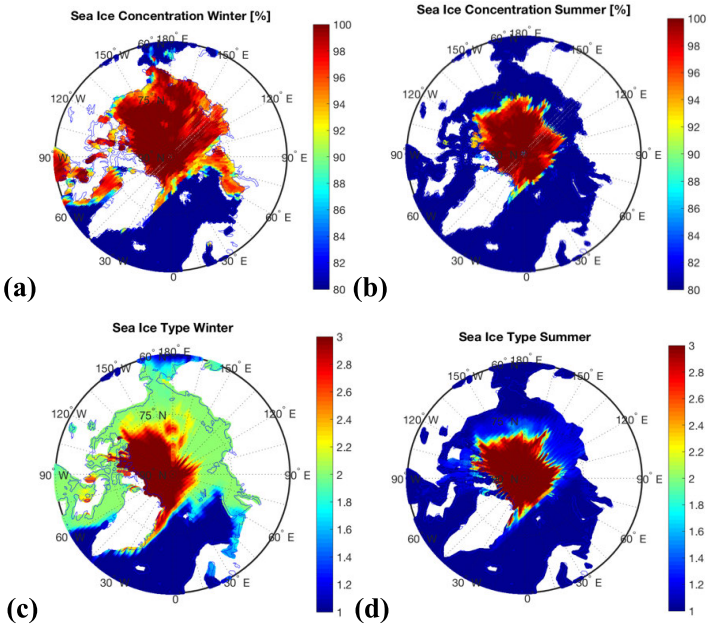

FIGURE 14. Sea ice concentration: (a) Winter, (b) Summer. Sea ice type: (c) Winter, (d) Summer. Data provided by the European Organisation for the Exploitation of Meteorological Satellites (EUMETSAT) Ocean and Sea Ice Satellite Application Facility (OSISAF). (1) no ice or vey open ice; (2) relatively young ice; (3) ice that survived a summer melt. Probability of miss-detection filtered out in data processing.

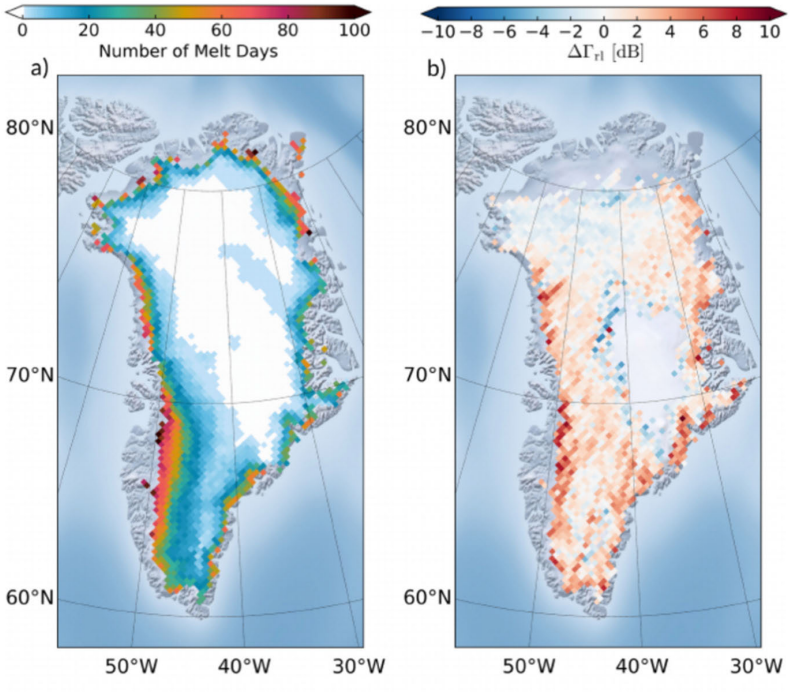

FIGURE 15. (a) The number of melt days over the Greenland ice sheet for each 25-km grid cell, which is accumulated from the Greenland daily microwave radiometer surface melt map during the 2018 melt season (May–October), and (b) the averaged changes in GNSS-R reflectivity for each grid cell computed with the UK TDS-1 data collected during the 2018 melt season (May–October) [174].

multi-step classification approach based on UK TDS-1 data and Synthetic Aperture Radar SAR-derived sea ice type maps [172].

3) GLACIERS

A GNSS-R experiment over Greenland ice sheet was performed from SMAP in 2017 [35] using several observables

FIGURE 16. Artist's view of a Spire GNSS-R CubeSat mission. Image credits Spire Global.

(SNR, polarimetric ratio, and trailing-edge). Two main conclusions were found: a) It is feasible to monitor melting on the ice sheet and the corresponding seasonal fluctuations, b) the spreading of the waveforms increases with the amount of dry ice because of the impact of the volume scattering term. Over dry ice, volume scattering and scattering at different layers could occur allowing the GNSS signals to penetrate the subsurface. These findings triggered the possibility of cryosphere monitoring using GNSS-R sensors from space. Several dedicated studies over Greenland have also been performed with data provided by the UK TDS-1 mission. In [173], the information contained in the DDMs were inverted to obtain altimetric estimates, and the retrieved height showed, as expected, significant discrepancy with the ice surface elevation corresponding to the topography given by National Snow and Ice Data Center (NSIDC) Geoscience Laser Altimeter System (GLAS) data from the Ice, Cloud, and land Elevation Satellite (ICESat-1). The difference between the GNSS-R derived surface height and the ice surface elevation was attributed to the penetration of the L- band signal into the ice-sheet. In 2020, ice-sheet melting occurrence was detected using the reflectivity increment from the empirical background reflectivity (Fig. 15) [174].

V. GNSS+R 2021 AND BEYOND

Continuing the series of GRSS-co-sponsored conferences, GNSS+R 2021 will be held in Beijing, China. GNSS+R 2021 will be an international forum for reporting and discussing recent achievements in GNSS-R and other signals of opportunity. The meeting will focus on the latest advances in GNSS-R theory and modeling, instrumentation, algorithms and applications in the field of ocean, land, and cryosphere remote sensing. The ''Standard for Spaceborne GNSS-R Data and Metadata Content'' working group will meet there to share our standard [11] with all the potential users in the community.

VI. SUMMARY AND OUTLOOK

Future advancements on satellite subsystems and retrieval algorithms will further explore the performance of GNSS-R to derive geophysical parameters of interest such as wind speed, ocean surface height, soil moisture content, biomass, inland water, and sea ice. As such, the GNSS-R standard is focused on the definition of the L1 parameters required for the generation of scientifically valuable products. We aim to provide a strong foundation for GNSS-R data to further explore and shift the limits of this technique, independently of constraints imposed by current limitations on geophysical parameters retrieval algorithms. In this article, an overview of the different GNSS-R techniques with a spaceborne application has been shown. Additionally, a description of the most common retrieval algorithms has demonstrated the wide range of scientific applications of GNSS-R over ocean, land, and cryosphere. On the other hand, we have compiled some available information on most of the existing GNSS-R receivers. The wide variety of techniques, algorithms, and instruments motivated the development of this working group.

The GNSS-R community has been growing rapidly during recent years. In the next decade, constellations of small satellites (Fig. 16) are expected to be launched into space, and works have also proposed larger missions [20]–[22] (Fig. 17). As such, we should plan future data sets so that valuable and inter-comparable products will result with a view to enable long-term stability and retrieval consistency in support of science and operational applications.

VII. ON-LINE RESOURCES

GNSS+R Bibliography, Institute of Space Sciences. Online available: https://www.ice.csic.es/personal/rius/gnss_r_bibliography/index.html

Cyclone Global Navigation Satellite System, University of Michigan. Online available https://clasp-research.engin.umich.edu/missions/cygnss/ (07/07/2020).

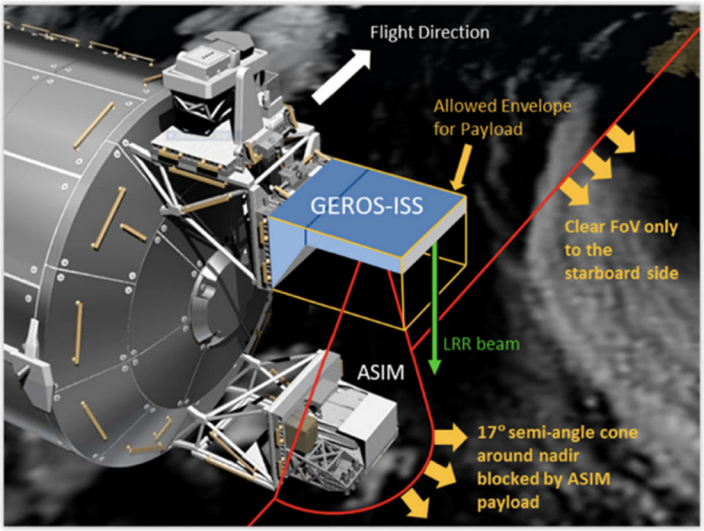

FIGURE 17. Artist's view of GEROS deployment at the upper Columbus External Payload Facility "upper balcony" of the ISS Columbus module with limited field of view [20].

PEPS/GEROS GNSS-R Simulator, Universitat Politecnica de Catalunya. Online available:
https://prs.upc.edu/2018/07/19/gnss-r-simulator/ (07/07/2020).

GEROS-SIM4LAND GNSS-R Simulator, Universitat Politecnica de Catalunya. Online available: http://147.83.91.189/ (07/07/2020).

P4003 - Standard for Global Navigation Satellite System-Reflectometry (GNSS-R) Data and Metadata Content, IEEE GRSS. Online available: https://standards.ieee.org/project/4003.html (07/07/2020).

APPENDIX: THE GNSS CONSTELLATIONS

An overview of the 4 GNSS constellations (Table 3) is provided in this Appendix. Understanding the heterogeneous nature of these signals of opportunity as well as the numerous types of constellations is important in the GNSS-R scenario.

A. GPS

GPS is a robust constellation consisting of 31 operational SVs plus 5 spares. More decommissioned satellites are in orbit and available as spares. Satellites are distributed over six orbital planes, separated by a Right Ascension of the Ascending Node (RAAN) of ∼60°, with an orbital inclination of ∼55°, and with an orbital radius of ∼26,600 km. Each satellite orbits the Earth twice every sidereal day, and the same ground track is repeated once per day. Therefore, the same constellation geometry can be observed every day with ∼4 minutes (235.909 seconds) difference. At the time of writing this article the constellation is composed of the following satellites: 9 GPS IIR transmitting the L1 C/A, L1 P(Y), and L2 P(Y) signals, 7 GPS IIRM transmitting the L1 C/A, L1 P(Y), L2 P(Y), L2C, L1M, and L2M signals, 12 GPS IIF transmitting the L1 C/A, L1 P(Y), L2 P(Y), L2C, L1M, L2M, and L5 signals, and 3 GPS IIIA transmitting the L1 C/A, L2 P(Y), L2C, L1M, L2M, and L5 signals. The GPS III satellites provide four civil signals, and they use 3 improved Rubidium atomic clocks. The GPS ground segment is composed by a primary master control station at Schriever Air Force Base (Colorado, USA), and 10 dedicated ground antennas and monitor stations.

B. GLONASSS

GLONASS was created by the Soviet Union and it became fully operational in 1995. Later, the constellation was reduced reaching a minimum of 8 operational satellites in 2002. However, since 2010 it is again fully operational and is currently composed of a total of 29 SVs from which 23 SVs are operational, 1 SV is in commissioning phase, 2 SVs are in maintenance, 1 SV is in flight tests phase, and 1 SV is a spare. GLONASS satellites orbit in three orbital planes inclined ∼64.8° and separated by ∼120°. Each plane includes 8 satellites equally spaced by ∼45°, and the orbital radius is of ∼25,511 km.

New SVs (GLONASS-K2) will improve the accuracy of current GLONASS-M and broaden the application domain. In particular, it is expected to achieve the following technical advantages: Longer guaranteed lifetime, modernization of SVs' support systems, improvement of on-board synchronizer stability, advanced technologies for monitoring and control, orbit and clock data provision, additional payloads and new signals (L1 OF, L2 OF, L1 SF, L2 SF, L1 OC, L1 SC, L2 OC, L2 SC, L3 OC). The first GLONASS-K2 launch took place in 2018. They are currently in testing phase. The key features of this new generation of satellites are the following:

- The SVs will allow the accommodation of all on-board specialized equipment without any restrictions.

TABLE 3. Parameters of the most common GNSS signals used in GNSS-R: GPS L1 C/A, GPS L2 P(Y), GPS L2 C, Galileo E1 OS, GLONASS C/A L1 and L2, GLONASS L2 P, and BeiDou B3I.

GNSS system	GPS	GPS	GPS	GPS	Galileo	GLONASS	GLONASS	GLONASS	BeiDou
Code name	C/A	P(Y)	CM	CL	E1 OS	C/A	C/A	P	B3I
Center Frequency (MHz)	1575.42	1227.6	1227.6	1227.6	1575.42	(1598.0625-1605.375) ± 0.511	(1242.93-1248.625) ± 0.511	(1242.93-1248.625 ± 0.511	1268.52
Frequency band	L1	L2	L2	L2	E1	L1	L2	L2	L2
Access technique	CDMA	CDMA	CDMA	CDMA	CDMA	FDMA	FDMA	FDMA	CDMA
Modulation	BPSK (1)	BPSK (10)	BPSK (1) results of multiplexing two streams of 511.5 kHz	BPSK (1) results of multiplexing two streams of 511.5 kHz	CBOC (6,1,1/11)	BPSK (0.511)	BPSK (0.511)	BPSK (0.511)	BPKS (10)
Sub-carrier frequency (MHz)	-	-	-	-	1.023 and 6.138 (Two sub-carriers)	-	-	-	-
Chipping rate (MHz)	1.023	10.23	0.5115	0.5115	1.023	0.511	0.511	0.511	10.23
Signal component	Data	Data	Data	Pilot	Data Pilot	Data	Data	Data	Data
Primary PRN code length	1023	6.19 x 1012	10230	767250	4092	511	511	-	10230
Code Family	Gold codes	Combination and short cycling of M sequences	M-sequence from a maximal polynomial of degree 27	M-sequence from a maximal polynomial of degree 27	Random Codes	M-sequences	M-sequences	-	-
Secondary PRN code length	-	-	-	-	25	-	-	-	-
Data rate	50 bps	50 bps	IIF 50 bps; IIR-M also 25 bps	NA	250 bps NA	50 bps	50 bps	250 bps	50
Minimum received power (dBW)	-158.5	II/IIA/IIR -164.5 IIR-M -161.4 IIF -160.0	II/IIA/IIR -164.5 IIR-M -161.5 IIF -161.5	-157	-157	-161	-167	-	-163

- The on-board subsystems will provide operational conditions for the specialized instruments without any constraints imposed by power consumption and thermal control.
- The maximum pointing error will be better than ∼0.25°.
- The Inter-Satellite Link (ISL) will allow continuous operation during one cycle (reception-transmission) without restrictions.
- Additional payloads to perform tests in space environment and to achieve flight qualification could be accommodated. The GLONASS ground control segment includes the deployment of a measuring station network in Russia and Antarctica, the deployment of an uplink station network in Russia, the deployment of a global measuring station outside Russia, and the further use of crosslink functions for ephemerides and clock data provision.

C. GALILEO

In March 2002, the European Union (EU) and the European Space Agency (ESA) agreed to develop the Galileo navigation system, which was expected to be fully functional by 2020. At the time of writing this document, Galileo is under development, and it will be fully compatible with the modernized GPS system. At present, GNSS receivers are able to combine signals from several constellations to increase significantly the achievable accuracy. As compared to the USA GPS and the Russian GLONASS, Galileo is designed specifically for civilian and commercial purposes. The In-Orbit Validation Element (GIOVE) A and B SVs, dedicated to take the first step of the in-orbit validation phase towards full deployment of Galileo, were launched in 2005 and 2008 respectively, and retired in 2012. Three In-Orbit Validation (IOV) SVs were launched from 2011 to 2012, being fully operational in 2015. At present, the Galileo

constellation is composed of 22 operational SVs from which 3 SVs are IOV type, 19 SVs are Full Operational Capability (FOC) type, 2 SVs are in testing phase, 2 SVs are unavailable, and 2 SVs have been retired. The full constellation will consist of 30 SVs, 24 SVs operational and 6 active spares, distributed in three orbital planes (∼56° inclination) with an orbital radius of ∼26,600 km and with an orbital period of ∼14 h.

Technology advances include:

- To improve robustness, quicker recovering from failures, and the Orbit Determination and Time Synchronization (ODTS) system, so as to provide long-term ephemerides. More specifically, improvements are required on Passive Hydrogen Maser (PHM), mini PHM, robust Rubidium Atomic Frequency Standard (RAFS) and cesium clocks.
- Increased SV capability while maintaining as a minimum the same launch cost efficiency (to confirm by testing the capability of state-of-the-art electric propulsion subsystems).
- Enabling either communication and/or ranging capabilities (in-plane and inter-plane ISL, ODTS exploiting ISL ranging, communication capabilities used for navigation message dissemination and for improving system robustness).
- The technology advances related to the improvement of the ODTS system are the following: Use of several faster navigation messages, improvement of orbit modelling, use of advanced navigation messages by means of Signal-In-Space (SIS) spare bits/words, d) enhancing fault detection mechanisms, and e) use of adaptive clock fitting.

D. BeiDou

BeiDou consists of 2 separate satellite constellations. The first BeiDou system, officially called the BeiDou Satellite Navigation Experimental System (BeiDou-1), consisted of 3 satellites. BeiDou-1 offered limited coverage and navigation services, mainly for users in China and neighboring regions. BeiDou-1 was decommissioned at the end of 2012. The second generation of the system, officially known as COMPASS or BeiDou-2, became operational in China in December 2011, with a partial constellation of 10 satellites in orbit. Since December 2012, it has been offering services to customers in the Asia-Pacific region (currently 15 operational SVs). In 2015, China launched the third generation of the BeiDou system (BeiDou-3) for global coverage. The first BeiDou-3 satellite was launched on March 30th 2015. On December 27th 2018, BeiDou-3 started providing global services, and the final satellite was launched into orbit on June 23th 2020.

BeiDou-3 is composed of a total of 34 SVs, 29 SVs operational, and 5 spares. BeiDou-3 utilizes high stability hydrogen atomic and rubidium clocks. Additionally, ISLs help with time synchronization, and enhance search & rescue services and Message Communication Services (MCS), including regional MCS and global short MCS. The Radio Determination Satellite Service (RDSS) payload of the Beidou-3G satellites consists of a high-power S-band transponder, a low-noise L-band amplifier and frequency generator, a phased array L-band antenna, a L-/S-band dish antenna and a C-band antenna. RDSS uses the original position retrieval including the central ground station to provide compatibility of the new system with existing BeiDou-1 terminals. On the other hand, the Radio Navigation Satellite Service (RNSS) payload uses ultra-stable timing signals delivered by an atomic clock to generate L-band signals that are transmitted through an antenna array. RNSS also includes an L-band uplink receiver and laser reflector for orbit determination. This payload works on the same principle as GPS and Galileo, using similar frequency bands.

REFERENCES

[1] H. Carreno-Luengo *et al.*, "The GRSS standard for GNSS-reflectometry," in *Proc. IEEE IGARSS*, Waikoloa, HI, USA, Jul. 2020, pp. 6289–6292.

[2] P. Jales and M. Unwin. *MERRByS Product Manual—GNSS Reflectometry on TDS-1 With the SGR-ReSI*. Accessed: Jul. 1, 2020. [Online]. Available: http://merrbys.co.uk/wp-content/uploads/2018/12/0248366_MERRByS-Product-Manual-GNSSReflectometry-on-TDS-1-with-the-SGR-ReSI-v005.pdf

[3] C. Ruf. *CYGNSS Handbook. Cyclone Global Navigation Satellite System*. Accessed: Jun. 20, 2020. [Online]. Available: https://clasp-research.engin.umich.edu/missions/cygnss/reference/cygnss-mission/CYGNSS_Handbook_April2016.pdf

[4] V. U. Zavorotny, S. Gleason, E. Cardellach, and A. Camps, "Tutorial on remote sensing using GNSS bistatic radar of opportunity," *IEEE Geosci. Remote Sens. Mag.*, vol. 2, no. 4, pp. 8–45, Dec. 2014.

[5] M. Martín-Neira, "A passive reflectometry and interferometry system (PARIS): Application to ocean altimetry," *ESA J.*, vol. 17, no. 4, pp. 331–355, 1993.

[6] H. Carreno-Luengo, A. Camps, J. Querol, and G. Forte, "First results of a GNSS-R experiment from a stratospheric balloon over boreal forests," *IEEE Trans. Geosci. Remote Sens.*, vol. 54, no. 5, pp. 2652–2663, May 2016.

[7] A. Alonso-Arroyo, A. Camps, H. Park, D. Pascual, R. Onrubia, and F. Martín, "Retrieval of significant wave height and mean sea surface level using the GNSS-R interference pattern technique: Results from a three-month field campaign," *IEEE Trans. Geosci. Remote Sens.*, vol. 53, no. 6, pp. 3198–3209, Jun. 2015.

[8] A. G. Voronovich and V. U. Zavorotny, "Bistatic radar equation for signals of opportunity revisited," *IEEE Trans. Geosci. Remote Sens.*, vol. 56, no. 4, pp. 1959–1968, Apr. 2018.

[9] H. Carreno-Luengo, G. Luzi, and M. Crosetto, "Sensitivity of CyGNSS bistatic reflectivity and SMAP microwave radiometry brightness temperature to geophysical parameters over land surfaces," *IEEE J. Sel. Topics Appl. Earth Observ. Remote Sens.*, vol. 12, no. 1, pp. 107–122, Jan. 2019.

[10] H. Carreno-Luengo, C. Ruf, A. Warnock, and K. Brunner, "Investigating the impact of coherent and incoherent scattering terms in GNSS-R delay Doppler maps," in *Proc. IEEE IGARSS*, Waikoloa, HI, USA, Sep. 2020, pp. 6202–6205.

[11] H. Carreno-Luengo *et al.*, *IEEE Standard for Global Navigation Satellite System-Reflectometry (GNSS-R) Data and Metadata Content*, Standard P4003, IEEE Standards Association, 2021.

[12] A. M. Semmling, V. Leister, J. Saynisch, F. Zus, S. Heise, and J. Wickert, "A phase-altimetric simulator: Studying the sensitivity of earth-reflected GNSS signals to ocean topography," *IEEE Trans. Geosci. Remote Sens.*, vol. 54, no. 11, pp. 6791–6802, Nov. 2016.

[13] V. A. Nguyen, O. Nogués-Correig, T. Yuasa, D. Masters, and V. Irisov, "Initial GNSS phase altimetry measurements from the spire satellite constellation," *Geophys. Res. Lett.*, vol. 47, no. 15, Aug. 2020, Art. no. e2020GL088308.

[14] M. Martin-Neira, S. D'Addio, C. Buck, N. Floury, and R. Prieto-Cerdeira, "The PARIS ocean altimeter in-orbit demonstrator," *IEEE Trans. Geosci. Remote Sens.*, vol. 49, no. 6, pp. 2209–2237, Jun. 2011.
[15] J. L. Garrison and S. J. Katzberg, "The application of reflected GPS signals to ocean remote sensing," *Remote Sens. Environ.*, vol. 73, no. 2, pp. 175–187, Aug. 2000.
[16] S. Gleason, C. S. Ruf, A. J. O'Brien, and D. S. McKague, "The CYGNSS level 1 calibration algorithm and error analysis based on on-orbit measurements," *IEEE J. Sel. Topics Appl. Earth Observ. Remote Sens.*, vol. 12, no. 1, pp. 37–49, Jan. 2019.
[17] T. Wang, C. S. Ruf, B. Block, D. S. McKague, and S. Gleason, "Design and performance of a GPS constellation power monitor system for improved CYGNSS L1B calibration," *IEEE J. Sel. Topics Appl. Earth Observ. Remote Sens.*, vol. 12, no. 1, pp. 26–36, Jan. 2019.
[18] D. Pascual, H. Park, R. Onrubia, A. A. Arroyo, J. Querol, and A. Camps, "Crosstalk statistics and impact in interferometric GNSS-R," *IEEE J. Sel. Topics Appl. Earth Observ. Remote Sens.*, vol. 9, no. 10, pp. 4621–4630, Oct. 2016.
[19] J. Querol, A. Alonso-Arroyo, R. Onrubia, D. Pascual, H. Park, and A. Camps, "SNR degradation in GNSS-R measurements under the effects of radio-frequency interference," *IEEE J. Sel. Topics Appl. Earth Observ. Remote Sens.*, vol. 9, no. 10, pp. 4865–4878, Oct. 2016.
[20] J. Wickert *et al.*, "GEROS-ISS: GNSS REflectometry, radio occultation, and scatterometry onboard the international space station," *IEEE J. Sel. Topics Appl. Earth Observ. Remote Sens.*, vol. 9, no. 10, pp. 4552–4581, Oct. 2016.
[21] E. Cardellach *et al.*, "GNSS transpolar earth reflectometry explori Ng system (G-TERN): Mission concept," *IEEE Access*, vol. 6, pp. 13980–14018, 2018.
[22] M. Martin-Neira, W. Li, A. Andres-Beivide, and X. Ballesteros-Sels, "Cookie: A satellite concept for GNSS remote sensing constellations," *IEEE J. Sel. Topics Appl. Earth Observ. Remote Sens.*, vol. 9, no. 10, pp. 4593–4610, Oct. 2016.
[23] A. Rius, O. Nogués-Correig, S. Ribó, E. Cardellach, S. Oliveras, E. Valencia, H. Park, J. M. Tarongí, A. Camps, H. van der Marel, R. van Bree, B. Altena, and M. Martín-Neira, "Altimetry with GNSS-R interferometry: First proof of concept experiment," *GPS Solutions*, vol. 16, no. 2, pp. 231–241, Apr. 2012.
[24] E. Cardellach, A. Rius, M. Martin-Neira, F. Fabra, O. Nogues-Correig, S. Ribo, J. Kainulainen, A. Camps, and S. D'Addio, "Consolidating the precision of interferometric GNSS-R ocean altimetry using airborne experimental data," *IEEE Trans. Geosci. Remote Sens.*, vol. 52, no. 8, pp. 4992–5004, Aug. 2014.
[25] F. Fabra, E. Cardellach, S. Ribó, W. Li, A. Rius, J. Arco-Fernández, O. Nogués-Correig, J. Praks, E. Rouhe, J. Seppänen, and M. Martín-Neira, "Is accurate synoptic altimetry achievable by means of interferometric GNSS-R?" *Remote Sens.*, vol. 11, no. 5, p. 505, Mar. 2019.
[26] R. Onrubia, D. Pascual, J. Querol, H. Park, and A. Camps, "The global navigation satellite systems reflectometry (GNSS-R) microwave interferometric reflectometer: Hardware, calibration, and validation experiments," *Sensors*, vol. 19, no. 5, p. 1019, Feb. 2019.
[27] H. Carreno-Luengo, A. Camps, I. Ramos-Perez, and A. Rius, "Experimental evaluation of GNSS-reflectometry altimetric precision using the P(Y) and C/A signals," *IEEE J. Sel. Topics Appl. Earth Observ. Remote Sens.*, vol. 7, no. 5, pp. 1493–1500, May 2014.
[28] S. T. Lowe, T. Meehan, and L. Young, "Direct signal enhanced semi-codeless processing of GNSS surface-reflected signals," *IEEE J. Sel. Topics Appl. Earth Observ. Remote Sens.*, vol. 7, no. 5, pp. 1469–1472, May 2014.
[29] W. Li, D. Yang, S. D'Addio, and M. Martin-Neira, "Partial interferometric processing of reflected GNSS signals for ocean altimetry," *IEEE Geosci. Remote Sens. Lett.*, vol. 11, no. 9, pp. 1509–1513, Sep. 2014.
[30] H. Park, E. Valencia, A. Camps, A. Rius, S. Ribo, and M. Martin-Neira, "Delay tracking in spaceborne GNSS-R ocean altimetry," *IEEE Geosci. Remote Sens. Lett.*, vol. 10, no. 1, pp. 57–61, Jan. 2013.
[31] H. Park, D. Pascual, A. Camps, F. Martin, A. Alonso-Arroyo, and H. Carreno-Luengo, "Analysis of spaceborne GNSS-R delay-Doppler tracking," *IEEE J. Sel. Topics Appl. Earth Observ. Remote Sens.*, vol. 7, no. 5, pp. 1481–1492, May 2014.
[32] S. Gleason, S. Hodgart, Y. Sun, C. Gommenginger, S. Mackin, M. Adjrad, and M. Unwin, "Detection and processing of bistatically reflected GPS signals from low earth orbit for the purpose of ocean remote sensing," *IEEE Trans. Geosci. Remote Sens.*, vol. 43, no. 6, pp. 1229–1241, Jun. 2005.
[33] M. Unwin, P. Jales, J. Tye, C. Gommenginger, G. Foti, and J. Rosello, "Spaceborne GNSS-reflectometry on TechDemoSat-1: Early mission operations and exploitation," *IEEE J. Sel. Topics Appl. Earth Observ. Remote Sens.*, vol. 9, no. 10, pp. 4525–4539, Oct. 2016.
[34] H. Carreno-Luengo, A. Camps, P. Vila, J. F. Munoz, A. Cortiella, D. Vidal, J. Jane, N. Catarino, M. Hagenfeldt, P. Palomo, and S. Cornara, "3Cat-2—An experimental nanosatellite for GNSS-R earth observation: Mission concept and analysis," *IEEE J. Sel. Topics Appl. Earth Observ. Remote Sens.*, vol. 9, no. 10, pp. 4540–4551, Oct. 2016.
[35] H. Carreno-Luengo, S. Lowe, C. Zuffada, S. Esterhuizen, and S. Oveisgharan, "Spaceborne GNSS-R from the SMAP mission: First assessment of polarimetric scatterometry over land and cryosphere," *Remote Sens.*, vol. 9, no. 4, p. 362, Apr. 2017.
[36] C. Jing, X. Niu, C. Duan, F. Lu, G. Di, and X. Yang, "Sea surface wind speed retrieval from the first Chinese GNSS-R mission: Technique and preliminary results," *Remote Sens.*, vol. 11, no. 24, p. 3013, Dec. 2019.
[37] D. Masters, "Design and planning for the first spire GNSS-R missions of 2019," in *Proc. IEEE GRSS, Spec. Meeting Reflectometry Using GNSS Other Signals Opportunity*, Benevento, Italy, May 2019.
[38] Y. Sun, Y. Tian, Y. Tian, C. Liu, W. Li, D. Zhao, F. Li, H. Qiao, X. Wang, Q. Du, W. Bai, J. Xia, Y. Cai, D. Wang, C. Wu, and X. Meng, "The status and progress of Fengyun-3E GNOS II mission for GNSS remote sensing," in *Proc. IEEE IGARSS*, Yokohama, Japan, Jul. 2019, pp. 5181–5184.
[39] A. Camps, A. Golkar, A. Gutierrez, J. A. R. de Azua, J. F. Munoz-Martin, L. Fernandez, C. Diez, A. Aguilella, S. Briatore, R. Akhtyamov, and N. Garzaniti, "FSSCAT, the 2017 copernicus masters' 'ESA Sentinel small satellite challenge' winner: A federated polar and soil moisture tandem mission based on 6U cubesats," in *Proc. IEEE IGARSS*, Valencia, Spain, Jul. 2018, pp. 8285–8287.
[40] J. F. Munoz-Martin, N. Miguelez, R. Castella, L. Fernandez, A. Solanellas, P. Via, and A. Camps, "3Cat-4: Combined GNSS-R, L-band radiometer with RFI mitigation, and AIS receiver for a I-unit cubesat based on software defined radio," in *Proc. IEEE IGARSS*, Valencia, Spain, Jul. 2018, pp. 1063–1066.
[41] A. Dielacher, H. Fragner, M. Moritsch, P. Høeg, J. Wickert, E. Cardellach, O. Koudelka, P. Beck, R. Walker, M. Martin-Neira, and F. P. Lissi, "The passive reflectometer on board of PRETTY," in *Proc. ESA ARSI+KEO Conf.*, Amsterdam, The Netherlands, Nov. 2019.
[42] J.-C. Juang, S.-H. Ma, and C.-T. Lin, "Study of GNSS-R techniques for FORMOSAT mission," *IEEE J. Sel. Topics Appl. Earth Observ. Remote Sens.*, vol. 9, no. 10, pp. 4582–4592, Oct. 2016.
[43] A. Helm, O. Montenbruck, J. Ashjaee, S. Yudanov, G. Beyerle, R. Stosius, and M. Rothacher, "GORS—A GNSS occultation, reflectometry and scatterometry space receiver," in *Proc. ION-GNSS Conf.*, Fort Worth, TX, USA, Sep. 2007, pp. 2011–2021.
[44] A. Helm, "Ground-based GPS altimetry with the L1 OpenGPS receiver using carrier phase-delay observations of reflected GPS signals," Deutsches GeoForschungsZentrum GFZ, Berlin, Germany, Tech. Rep. STR 08/10, 2008.
[45] M. Unwin, P. Jales, P. Blunt, S. Duncan, M. Brummitt, and C. Ruf, "The SGR-ReSI and its application for GNSS reflectometry on the NASA EV-2 CYGNSS mission," in *Proc. IEEE Aerosp. Conf.*, Big Sky, MT, USA, Mar. 2013, pp. 1–6.
[46] C. Ruf, R. Backhus, T. Butler, C.-C. Chen, S. Gleason, E. Loria, D. McKague, R. Miller, A. O'Brien, and L. van Nieuwstadt, "Next generation GNSS-R instrument," in *Proc. IEEE IGARSS*, Waikoloa, HI, USA, Sep. 2020, pp. 3353–3356.
[47] E. Motte, M. Zribi, P. Fanise, A. Egido, J. Darrozes, A. Al-Yaari, N. Baghdadi, F. Baup, S. Dayau, R. Fieuzal, P.-L. Frison, D. Guyon, and J.-P. Wigneron, "GLORI: A GNSS-R dual polarization airborne instrument for land surface monitoring," *Sensors*, vol. 16, no. 5, p. 732, May 2016.
[48] O. Nogues-Correig, E. C. Gali, J. S. Campderros, and A. Rius, "A GPS-reflections receiver that computes Doppler/delay maps in real time," *IEEE Trans. Geosci. Remote Sens.*, vol. 45, no. 1, pp. 156–174, Jan. 2007.
[49] A. Rius, F. Fabra, S. Ribo, J. C. Arco, S. Oliveras, E. Cardellach, A. Camps, O. Nogues-Correig, J. Kainulainen, E. Rohue, and M. Martin-Neira, "PARIS interferometric technique proof of concept: Sea surface altimetry measurements," in *Proc. IEEE Int. Geosci. Remote Sens. Symp.*, Munich, Germany, Jul. 2012, pp. 7067–7070.

[50] S. Ribó, J. Arco-Fernández, E. Cardellach, F. Fabra, W. Li, O. Nogués-Correig, A. Rius, and M. Martín-Neira, "A software-defined GNSS reflectometry recording receiver with wide-bandwidth, multi-band capability and digital beam-forming," *Remote Sens.*, vol. 9, no. 5, p. 450, May 2017.

[51] O. Nogues-Correig, "Disseny, Montatge i Validacio d'un Receptor/Gravador de Senyals GPS per a la Demostracio del Concepte PARIS," Proyecto Final Carrera, Univ. Politecnica Catalunya, Barcelona, Spain, Tech. Rep., 2002.

[52] O. Nogues, A. Sumpsi, A. Camps, and A. Rius, "A 3 GPS-channels Doppler-delay receiver for remote sensing applications," in *Proc. IEEE IGARSS*, Toulouse, France, Sep. 2003, pp. 4483–4485.

[53] N. Rodriguez-Alvarez, X. Bosch-Lluis, A. Camps, M. Vall-Llossera, E. Valencia, J. F. Marchan-Hernandez, and I. Ramos-Perez, "Soil moisture retrieval using GNSS-R techniques: Experimental results over a bare soil field," *IEEE Trans. Geosci. Remote Sens.*, vol. 47, no. 11, pp. 3616–3624, Nov. 2009.

[54] R. Olive, A. Amezaga, H. Carreno-Luengo, H. Park, and A. Camps, "Implementation of a GNSS-R payload based on software-defined radio for the 3CAT-2 mission," *IEEE J. Sel. Topics Appl. Earth Observ. Remote Sens.*, vol. 9, no. 10, pp. 4824–4833, Oct. 2016.

[55] J. F. Munoz-Martin, L. F. Capon, J. A. Ruiz-de-Azua, and A. Camps, "The flexible microwave payload-2: A SDR-based GNSS-reflectometer and L-band radiometer for CubeSats," *IEEE J. Sel. Topics Appl. Earth Observ. Remote Sens.*, vol. 13, pp. 1298–1311, 2020.

[56] C. Ruf, "Mission update," in *Proc. CYGNSS Sci. Team Meeting*, Jun. 2020.

[57] M. Martin-Neira, M. Caparrini, J. Font-Rossello, S. Lannelongue, and C. S. Vallmitjana, "The PARIS concept: An experimental demonstration of sea surface altimetry using GPS reflected signals," *IEEE Trans. Geosci. Remote Sens.*, vol. 39, no. 1, pp. 142–150, Jan. 2001.

[58] S. T. Lowe, C. Zuffada, Y. Chao, P. Kroger, L. E. Young, and J. L. LaBrecque, "5-cm-precision aircraft ocean altimetry using GPS reflections," *Geophys. Res. Lett.*, vol. 29, no. 10, p. 1375, 2002.

[59] A. Rius, E. Cardellach, and M. Martin-Neira, "Altimetric analysis of the sea-surface GPS-reflected signals," *IEEE Trans. Geosci. Remote Sens.*, vol. 48, no. 4, pp. 2119–2127, Apr. 2010.

[60] S. D'Addio, M. Martin-Neira, M. di Bisceglie, C. Galdi, and F. M. Alemany, "GNSS-R altimeter based on Doppler multi-looking," *IEEE J. Sel. Topics Appl. Earth Observ. Remote Sens.*, vol. 7, no. 5, pp. 1452–1460, May 2014.

[61] A. M. Semmling, T. Schmidt, J. Wickert, S. Schön, F. Fabra, E. Cardellach, and A. Rius, "On the retrieval of the specular reflection in GNSS carrier observations for ocean altimetry," *Radio Sci.*, vol. 47, no. 6, Dec. 2012, Art. no. RS6007.

[62] A. M. Semmling, J. Beckheinrich, J. Wickert, G. Beyerle, S. Schön, F. Fabra, H. Pflug, K. He, J. Schwabe, and M. Scheinert, "Sea surface topography retrieved from GNSS reflectometry phase data of the GEO-HALO flight mission," *Geophys. Res. Lett.*, vol. 41, no. 3, pp. 954–960, Feb. 2014.

[63] A. M. Semmling, J. Wickert, S. Schön, R. Stosius, M. Markgraf, T. Gerber, M. Ge, and G. Beyerle, "A zeppelin experiment to study airborne altimetry using specular global navigation satellite system reflections," *Radio Sci.*, vol. 48, no. 4, pp. 427–440, Jul. 2013.

[64] E. Cardellach, C. O. Ao, M. de la Torre Juárez, and G. A. Hajj, "Carrier phase delay altimetry with GPS-reflection/occultation interferometry from low earth orbiters," *Geophys. Res. Lett.*, vol. 31, no. 10, pp. 1–4, May 2004.

[65] W. Li, E. Cardellach, F. Fabra, A. Rius, S. Ribó, and M. Martín-Neira, "First spaceborne phase altimetry over sea ice using TechDemoSat-1 GNSS-R signals," *Geophys. Res. Lett.*, vol. 44, no. 16, pp. 8369–8376, Aug. 2017.

[66] E. Cardellach, W. Li, A. Rius, M. Semmling, J. Wickert, F. Zus, C. S. Ruf, and C. Buontempo, "First precise spaceborne sea surface altimetry with GNSS reflected signals," *IEEE J. Sel. Topics Appl. Earth Observ. Remote Sens.*, vol. 13, pp. 102–112, 2020.

[67] M. P. Clarizia, C. Ruf, P. Cipollini, and C. Zuffada, "First spaceborne observation of sea surface height using GPS-reflectometry," *Geophys. Res. Lett.*, vol. 43, no. 2, pp. 767–774, Jan. 2016.

[68] W. Li, E. Cardellach, F. Fabra, S. Ribo, and A. Rius, "Assessment of spaceborne GNSS-R ocean altimetry performance using CYGNSS mission raw data," *IEEE Trans. Geosci. Remote Sens.*, vol. 58, no. 1, pp. 238–250, Jan. 2020.

[69] J. Mashburn, P. Axelrad, C. Zuffada, E. Loria, A. O'Brien, and B. Haines, "Improved GNSS-R ocean surface altimetry with CYGNSS in the seas of Indonesia," *IEEE Trans. Geosci. Remote Sens.*, vol. 58, no. 9, pp. 6071–6087, Sep. 2020.

[70] A. Ghavidel and A. Camps, "Time-domain statistics of the electromagnetic bias in GNSS-reflectometry," *Remote Sens.*, vol. 7, no. 9, pp. 11151–11162, Aug. 2015.

[71] A. Ghavidel, D. Schiavulli, and A. Camps, "Numerical computation of the electromagnetic bias in GNSS-R altimetry," *IEEE Trans. Geosci. Remote Sens.*, vol. 54, no. 1, pp. 489–498, Jan. 2016.

[72] A. Ghavidel and A. Camps, "Impact of rain, swell, and surface currents on the electromagnetic bias in GNSS-reflectometry," *IEEE J. Sel. Topics Appl. Earth Observ. Remote Sens.*, vol. 9, no. 10, pp. 4643–4649, Oct. 2016.

[73] F. Martin, A. Camps, H. Park, S. DaAddio, M. Martin-Neira, and D. Pascual, "Cross-correlation waveform analysis for conventional and interferometric GNSS-R approaches," *IEEE J. Sel. Topics Appl. Earth Observ. Remote Sens.*, vol. 7, no. 5, pp. 1560–1572, May 2014.

[74] S. J. Katzberg, R. A. Walker, J. H. Roles, T. Lynch, and P. G. Black, "First GPS signals reflected from the interior of a tropical storm: Preliminary results from hurricane Michael," *Geophys. Res. Lett.*, vol. 28, no. 10, pp. 1981–1984, May 2001.

[75] J. L. Garrison, A. Komjathy, V. U. Zavorotny, and S. J. Katzberg, "Wind speed measurement using forward scattered GPS signals," *IEEE Trans. Geosci. Remote Sens.*, vol. 40, no. 1, pp. 50–75, Jan. 2002.

[76] E. Cardellach, G. Ruffini, D. Pino, A. Rius, A. Komjathy, and J. L. Garrison, "Mediterranean balloon experiment: Ocean wind speed sensing from the stratosphere, using GPS reflections," *Remote Sens. Environ.*, vol. 88, no. 3, pp. 351–362, Dec. 2003.

[77] O. Germain, G. Ruffini, F. Soulat, M. Caparrini, B. Chapron, and P. Silvestrin, "The eddy experiment: GNSS-R speculometry for directional sea-roughness retrieval from low altitude aircraft," *Geophys. Res. Lett.*, vol. 31, no. 21, Nov. 2004, Art. no. L21307.

[78] M. P. Clarizia, C. P. Gommenginger, S. T. Gleason, M. A. Srokosz, C. Galdi, and M. Di Bisceglie, "Analysis of GNSS-R delay-Doppler maps from the UK-DMC satellite over the ocean," *Geophys. Res. Lett.*, vol. 36, no. 2, pp. 1–5, Jan. 2009.

[79] V. U. Zavorotny and A. G. Voronovich, "Scattering of GPS signals from the ocean with wind remote sensing application," *IEEE Trans. Geosci. Remote Sens.*, vol. 38, no. 2, pp. 951–964, Mar. 2000.

[80] T. Elfouhaily, D. R. Thompson, and L. Linstrom, "Delay-Doppler analysis of bistatically reflected signals from the ocean surface: Theory and application," *IEEE Trans. Geosci. Remote Sens.*, vol. 40, no. 3, pp. 560–573, Mar. 2002.

[81] S. Gleason, "Remote sensing of ocean, ice, and land surfaces using bistatically scattered GNSS signals from low earth orbit," Ph.D. dissertation, Univ. Surrey, Guildford, U.K., 2006.

[82] A. Camps, M. Caparrini, R. Sabia, and G. Ruffini, "Sea surface salinity retrieval from space: Potential synergetic use of GNSS-R signals to improve the sea state correction and application to the SMOS mission," in *Proc. IEEE Microw. Radiometry Remote Sens. Environ. (MicroRad)*, Feb. 2006, pp. 91–96.

[83] J. F. Marchan-Hernandez, N. Rodriguez-Alvarez, A. Camps, X. Bosch-Lluis, I. Ramos-Perez, and E. Valencia, "Correction of the sea state impact in the L-band brightness temperature by means of delay-Doppler maps of global navigation satellite signals reflected over the sea surface," *IEEE Trans. Geosci. Remote Sens.*, vol. 46, no. 10, pp. 2914–2923, Oct. 2008.

[84] E. Valencia, A. Camps, N. Rodriguez-Alvarez, I. Ramos-Perez, X. Bosch-Lluis, and H. Park, "Improving the accuracy of sea surface salinity retrieval using GNSS-R data to correct the sea state effect," *Radio Sci.*, vol. 46, no. 6, pp. 1–11, Dec. 2011.

[85] E. Cardellach and A. Rius, "A new technique to sense non-Gaussian features of the sea surface from L-band bi-static GNSS reflections," *Remote Sens. Environ.*, vol. 112, no. 6, pp. 2927–2937, Jun. 2008.

[86] E. Valencia, A. Camps, J. F. Marchan-Hernandez, H. Park, X. Bosch-Lluis, N. Rodriguez-Alvarez, and I. Ramos-Perez, "Ocean surface's scattering coefficient retrieval by delay-Doppler map inversion," *IEEE Geosci. Remote Sens. Lett.*, vol. 8, no. 4, pp. 750–754, Jul. 2011.

[87] G. Schiavulli, D. Nunziata, F. Pugliano, and M. Migliaccio, "Reconstruction of the normalized radar cross section field from GNSS-R delay Doppler map," *IEEE J. Sel. Topics Appl. Earth Observ. Remote Sens.*, vol. 7, no. 5, pp. 1573–1583, May 2014.

[88] G. Foti, C. Gommenginger, P. Jales, M. Unwin, A. Shaw, C. Robertson, and J. Roselló, "Spaceborne GNSS reflectometry for ocean winds: First results from the UK TechDemoSat-1 mission," *Geophys. Res. Lett.*, vol. 42, no. 13, pp. 5435–5441, Jul. 2015.
[89] B. Annane, B. McNoldy, S. Leidner, R. Hoffman, R. Atlas, and S. Majumdar, "A study of the HWRF analysis and forecast impact of realistically simulated CYGNSS observations assimilated as scalar wind speeds and as VAM wind vectors," *Monthly Weather Rev.*, vol. 146, no. 7, pp. 26–36, 2018.
[90] S. M. Leidner, B. Annane, B. McNoldy, R. Hoffman, and R. Atlas, "Variational analysis of simulated ocean surface winds from the cyclone global navigation satellite system (CYGNSS) and evaluation using a regional OSSE," *J. Atmos. Ocean. Technol.*, vol. 35, no. 8, pp. 1571–1584, Aug. 2018.
[91] Z. Cui, Z. Pu, V. Tallapragada, R. Atlas, and C. S. Ruf, "Impact of CYGNSS ocean surface wind speeds on numerical simulations of hurricanes Harvey and Irma (2017)," *Geophys. Res. Lett.*, vol. 46, no. 5, pp. 2984–2992, 2019.
[92] D. Mayers and C. Ruf, "Tropical cyclone center fix using CYGNSS winds," *J. Appl. Meteorol. Climatol.*, vol. 58, no. 9, pp. 1993–2003, Sep. 2019.
[93] M. P. Clarizia and C. S. Ruf, "Wind speed retrieval algorithm for the cyclone global navigation satellite system (CYGNSS) mission," *IEEE Trans. Geosci. Remote Sens.*, vol. 54, no. 8, pp. 4419–4432, Aug. 2016.
[94] C. S. Ruf, R. Atlas, P. S. Chang, M. P. Clarizia, J. L. Garrison, S. Gleason, S. J. Katzberg, Z. Jelenak, J. T. Johnson, S. J. Majumdar, A. O'Brien, D. J. Posselt, A. J. Ridley, R. J. Rose, and V. U. Zavorotny, "New ocean winds satellite mission to probe hurricanes and tropical convection," *Bull. Amer. Meteorol. Soc.*, vol. 97, no. 3, pp. 385–395, Mar. 2016.
[95] C. S. Ruf and R. Balasubramaniam, "Development of the CYGNSS geophysical model function for wind speed," *IEEE J. Sel. Topics Appl. Earth Observ. Remote Sens.*, vol. 12, no. 1, pp. 66–77, Jan. 2019.
[96] C. Ruf, S. Asharaf, R. Balasubramaniam, S. Gleason, T. Lang, D. McKague, D. Twigg, and D. Waliser, "In-orbit performance of the constellation of CYGNSS hurricane satellites," *Bull. Amer. Meteorol. Soc.*, vol. 100, no. 10, pp. 1–46, 2019.
[97] S. Gleason, C. S. Ruf, A. J. O'Brien, and D. S. McKague, "The CYGNSS level 1 calibration algorithm and error analysis based on on-orbit measurements," *IEEE J. Sel. Topics Appl. Earth Observ. Remote Sens.*, vol. 12, no. 1, pp. 37–49, Jan. 2019.
[98] J. Reynolds, M. P. Clarizia, and E. Santi, "Wind speed estimation from CYGNSS using artificial neural networks," *IEEE J. Sel. Topics Appl. Earth Observ. Remote Sens.*, vol. 13, pp. 708–716, 2020.
[99] M. P. Clarizia, "Investigating the effect of ocean waves on GNSS-R microwave remote sensing measurements," Ph.D. dissertation, School Ocean Earth Sci., Univ. Southampton, Southampton, U.K., 2012.
[100] H. Carreno-Luengo, A. Camps, I. Perez-Ramos, G. Forte, R. Onrubia, and R. Diez, "3Cat-2: A P(Y) and C/A GNSS-R experimental nano-satellite mission," in *Proc. IEEE IGARSS*, Melbourne, VIC, Australia, Jul. 2013, pp. 843–846.
[101] H. Carreno-Luengo and A. Camps, "Empirical results of a surface-level GNSS-R experiment in a wave channel," *Remote Sens.*, vol. 7, no. 6, pp. 7471–7493, Jun. 2015.
[102] S. Soisuvarn, Z. Jelenak, F. Said, P. S. Chang, and A. Egido, "The GNSS reflectometry response to the ocean surface winds and waves," *IEEE J. Sel. Topics Appl. Earth Observ. Remote Sens.*, vol. 9, no. 10, pp. 4678–4699, Oct. 2016.
[103] J. F. Munoz-Martin, R. Onrubia, D. Pascual, H. Park, A. Camps, C. Rudiger, J. Walker, and A. Monerris, "Untangling the incoherent and coherent scattering components in GNSS-R and novel applications," *Remote Sens.*, vol. 12, no. 7, p. 1018, 2020.
[104] J. F. Munoz-Martin, R. Onrubia, D. Pascual, H. Park, A. Camps, C. Rüdiger, J. Walker, and A. Monerris, "Experimental evidence of swell signatures in airborne L5/E5a GNSS-reflectometry," *Remote Sens.*, vol. 12, no. 11, p. 1759, May 2020.
[105] B. Li, L. Yang, B. Zhang, D. Yang, and D. Wu, "Modeling and simulation of GNSS-R observables with effects of swell," *IEEE J. Sel. Topics Appl. Earth Observ. Remote Sens.*, vol. 13, pp. 1833–1841, 2020.
[106] G. Carrie, T. Deloues, J. Mametsa, and S. Angelliaume, "Ship detection based on GNSS reflected signals: An experimental plan," in *Proc. Space Reflecto*, Calais, France, 2011.
[107] M. P. Clarizia, P. Braca, C. S. Ruf, and P. Willett, "Target detection using GPS signals of opportunity," in *Proc. 18th Int. Conf. Inf. Fusion*, Washington, DC, USA, 2015, pp. 1429–1436.
[108] W. Ji, C. Xiu, W. Li, and L. Wang, "Ocean surface target detection and positioning using the spaceborne GNSS-R delay-Doppler maps," in *Proc. IEEE IGARSS*, Quebec City, QC, Canada, Jul. 2014, pp. 3806–3809.
[109] Y. Lu, D. Yang, W. Li, J. Ding, and Z. Li, "Study on the new methods of ship object detection based on GNSS reflection," *Mar. Geodesy*, vol. 36, no. 1, pp. 22–30, Mar. 2013.
[110] A. Di Simone, H. Park, D. Riccio, and A. Camps, "Sea target detection using spaceborne GNSS-R delay-Doppler maps: Theory and experimental proof of concept using TDS-1 data," *IEEE J. Sel. Topics Appl. Earth Observ. Remote Sens.*, vol. 10, no. 9, pp. 4255–4537, Sep. 2017.
[111] B. J. Southwell, J. W. Cheong, and A. G. Dempster, "A matched filter for spaceborne GNSS-R based sea-target detection," *IEEE Trans. Geosci. Remote Sens.*, vol. 58, no. 8, pp. 5922–5931, Aug. 2020.
[112] T. Beltramont, P. Braca, M. Di Bisceglie, A. Di Simone, C. Galdi, A. Iodice, L. M. Millefiori, D. Riccio, and P. Willett, "Simulation-based feasibility analysis of ship detection using GNSS-R delay-Doppler maps," *IEEE J. Sel. Topics Appl. Earth Observ. Remote Sens.*, vol. 10, no. 9, pp. 4255–4537, Mar. 2020.
[113] D. Masters, V. Zavorotny, S. Katzberg, and W. Emery, "GPS signal scattering from land for moisture content determination," in *Proc. IEEE IGARSS*, Honolulu, HI, USA, Jul. 2000, pp. 3090–3092.
[114] A. Egido, C. Martin-Puig, D. Felip, M. Garcia, M. Caparrini, E. Farres, and G. Ruffini, "The SAM sensor: An innovative GNSS-R system for soil moisture retrieval," in *Proc. NAVITEC Conf. Eur. Space Technol. Centre (ESTEC/ESA)*, Noordwijk, The Netherlands, Apr. 2008.
[115] S. J. Katzberg, O. Torres, M. S. Grant, and D. Masters, "Utilizing calibrated GPS reflected signals to estimate soil reflectivity and dielectric constant: Results from SMEX02," *Remote Sens. Environ.*, vol. 100, no. 1, pp. 17–28, Jan. 2006.
[116] N. Pierdicca, L. Guerriero, R. Giusto, M. Brogioni, and A. Egido, "SAVERS: A simulator of GNSS reflections from bare and vegetated soils," *IEEE Trans. Geosci. Remote Sens.*, vol. 52, no. 10, pp. 6542–6554, Oct. 2014.
[117] V. U. Zavorotny, K. M. Larson, J. J. Braun, E. E. Small, E. D. Gutmann, and A. L. Bilich, "A physical model for GPS multipath caused by land reflections: Toward bare soil moisture retrievals," *IEEE J. Sel. Topics Appl. Earth Observ. Remote Sens.*, vol. 3, no. 1, pp. 100–110, Mar. 2010.
[118] K. M. Larson, E. E. Small, E. Gutmann, A. Bilich, P. Axelrad, and J. Braun, "Using GPS multipath to measure soil moisture fluctuations: Initial results," *GPS Solutions*, vol. 12, no. 3, pp. 173–177, Jul. 2008.
[119] A. A. Arroyo, A. Camps, A. Aguasca, G. F. Forte, A. Monerris, C. Rudiger, J. P. Walker, H. Park, D. Pascual, and R. Onrubia, "Dual-polarization GNSS-R interference pattern technique for soil moisture mapping," *IEEE J. Sel. Topics Appl. Earth Observ. Remote Sens.*, vol. 7, no. 5, pp. 1533–1544, May 2014.
[120] A. Egido, S. Paloscia, E. Motte, L. Guerriero, N. Pierdicca, M. Caparrini, E. Santi, G. Fontanelli, and N. Floury, "Airborne GNSS-R polarimetric measurements for soil moisture and above-ground biomass estimation," *IEEE J. Sel. Topics Appl. Earth Observ. Remote Sens.*, vol. 7, no. 5, pp. 1522–1532, May 2014.
[121] E. Motte, M. Zribi, P. Fanise, A. Egido, J. Darrozes, A. Al-Yaari, N. Baghdadi, F. Baup, S. Dayau, R. Fieuzal, P.-L. Frison, D. Guyon, and J.-P. Wigneron, "GLORI: A GNSS-R dual polarization airborne instrument for land surface monitoring," *Sensors*, vol. 16, no. 5, p. 732, May 2016.
[122] E. E. Small, K. M. Larson, C. C. Chew, J. Dong, and T. E. Ochsner, "Validation of GPS-IR soil moisture retrievals: Comparison of different algorithms to remove vegetation effects," *IEEE J. Sel. Topics Appl. Earth Observ. Remote Sens.*, vol. 9, no. 10, pp. 4759–4770, Oct. 2016.
[123] A. Camps, H. Hyuk, M. Pablos, G. Foti, C. Gommerginger, P. W. Liu, and J. Judge, "Sensitivity of GNSS-R spaceborne observations to soil moisture and vegetation," *IEEE J. Sel. Topics Appl. Earth Observ. Remote Sens.*, vol. 9, no. 10, pp. 4730–4732, Oct. 2016.
[124] C. Chew, R. Shah, C. Zuffada, G. Hajj, D. Masters, and A. J. Mannucci, "Demonstrating soil moisture remote sensing with observations from the UK TechDemoSat-1 satellite mission," *Geophys. Res. Lett.*, vol. 43, no. 7, pp. 3317–3324, Apr. 2016.
[125] M. Piles, D. Entekhabi, A. G. Konings, K. A. McColl, N. N. Das, and T. Jagdhuber, "Multi-temporal microwave retrievals of soil moisture and vegetation parameters from SMAP," in *Proc. IEEE IGARSS*, Beijing, China, Jul. 2016, pp. 202–245.
[126] C. C. Chew and E. E. Small, "Soil moisture sensing using spaceborne GNSS reflections: Comparison of CYGNSS reflectivity to SMAP soil moisture," *Geophys. Res. Lett.*, vol. 45, no. 9, pp. 4049–4057, May 2018.

[127] H. Carreno-Luengo, G. Luzi, and M. Crosetto, "Impact of the elevation angle on CYGNSS GNSS-bistatic reflectivity," *Remote Sens.*, vol. 10, no. 11, pp. 1–21, 2018.

[128] A. Camps, M. Vall-Llossera, H. Park, G. Portal, and L. Rossato, "Sensitivity of TDS-1 GNSS-R reflectivity to soil moisture: Global and regional differences and impact of different spatial scales," *Remote Sens.*, vol. 10, no. 11, p. 1856, Nov. 2018.

[129] M. M. Al-Khaldi, J. T. Johnson, A. J. O'Brien, A. Balenzano, and F. Mattia, "Time-series retrieval of soil moisture using CYGNSS," *IEEE Trans. Geosci. Remote Sens.*, vol. 57, no. 7, pp. 4322–4331, Jul. 2019.

[130] M. P. Clarizia, N. Pierdicca, F. Costantini, and N. Floury, "Analysis of CYGNSS data for soil moisture retrieval," *IEEE J. Sel. Topics Appl. Earth Observ. Remote Sens.*, vol. 12, no. 7, pp. 2227–2235, Jul. 2019.

[131] C. Chew and E. Small, "Description of the UCAR/CU soil moisture product," *Remote Sens.*, vol. 12, no. 10, p. 1558, May 2020.

[132] A. Camps, H. Park, J. Castellví, J. Corbera, and E. Ascaso, "Single-pass soil moisture retrievals using GNSS-R: Lessons learned," *Remote Sens.*, vol. 12, no. 12, p. 2064, Jun. 2020.

[133] H. Park, A. Camps, J. Castellvi, and J. Muro, "Generic performance simulator of spaceborne GNSS-reflectometer for land applications," *IEEE J. Sel. Topics Appl. Earth Observ. Remote Sens.*, vol. 13, pp. 3179–3191, 2020.

[134] P. Liang, L. E. Pierce, and M. Moghaddam, "Radiative transfer model for microwave bistatic scattering from forest canopies," *IEEE Trans. Geosci. Remote Sens.*, vol. 43, no. 11, pp. 2470–2483, Nov. 2005.

[135] P. Ferrazzoli, L. Guerriero, N. Pierdicca, and R. Rahmoune, "Forest biomass monitoring with GNSS-R: Theoretical simulations," *Adv. Space Res.*, vol. 47, no. 10, pp. 1823–1832, May 2011.

[136] X. R. Wu and S. J. Jin, "GPS-reflectometry: Forest canopies polarization scattering properties and modelling," *Adv. Space Res.*, vol. 54, no. 5, pp. 863–870, 2014.

[137] A. Egido, "GNSS refectometry for land remote sensing applications," Ph.D. dissertation, Univ. Politecnica Catalunya, Barcelona, Spain, 2013. Accessed: May 1, 2020. [Online]. Available: https://tdx.cat/handle/10803/129090

[138] H. Carreno-Luengo, "Contributions to GNSS-R earth remote sensing from nano-satellites," Ph.D. dissertation, Univ. Politecnica Catalunya, Barcelona, Spain, 2016. Accessed: May 1, 2020. [Online]. Available: https://www.tdx.cat/handle/10803/385216

[139] H. Carreno-Luengo, A. Amèzaga, D. Vidal, R. Olivé, J. Munoz, and A. Camps, "First polarimetric GNSS-R measurements from a stratospheric flight over boreal forests," *Remote Sens.*, vol. 7, no. 10, pp. 13120–13138, Oct. 2015.

[140] M. Kurum, M. Deshpande, A. T. Joseph, P. E. O'Neill, R. H. Lang, and O. Eroglu, "SCoBi-veg: A generalized bistatic scattering model of reflectometry from vegetation for signals of opportunity applications," *IEEE Trans. Geosci. Remote Sens.*, vol. 57, no. 2, pp. 1049–1068, Feb. 2019.

[141] A. Lindenmayer, "Developmental algorithms for multicellular organisms: A survey of L-systems," *J. Theor. Biol.*, vol. 54, no. 1, pp. 3–22, Jan. 1975.

[142] L. Tsang, J. A. Kong, and R. T. Shin, *Theory of Microwave Remote Sensing*. New York, NY, USA: Wiley, 1985.

[143] M. Zribi, D. Guyon, E. Motte, S. Dayau, J. P. Wigneron, N. Baghdadi, and N. Pierdicca, "Performance of GNSS-R GLORI data for biomass estimation over the landes forest," *Int. J. Appl. Earth Observ. Geoinf.*, vol. 74, pp. 150–158, Feb. 2019.

[144] H. Carreno-Luengo, G. Luzi, and M. Crosetto, "Above-ground biomass retrieval over tropical forests: A novel GNSS-R approach with CyGNSS," *Remote Sens.*, vol. 12, no. 9, p. 1368, Apr. 2020.

[145] A. Camps, A. Alonso-Arroyo, H. Park, R. Onrubia, D. Pascual, and J. Querol, "L-band vegetation optical depth estimation using transmitted GNSS signals: Application to GNSS-reflectometry and positioning," *Remote Sens.*, vol. 12, no. 15, p. 2352, Jul. 2020.

[146] S. V. Nghiem, C. Zuffada, R. Shah, C. Chew, S. T. Lowe, A. J. Mannucci, E. Cardellach, G. R. Brakenridge, G. Geller, and A. Rosenqvist, "Wetland monitoring with global navigation satellite system reflectometry," *Earth Space Sci.*, vol. 4, no. 1, pp. 16–39, Jan. 2017.

[147] C. Chew, J. T. Reager, and E. Small, "CYGNSS data map flood inundation during the 2017 Atlantic hurricane season," *Sci. Rep.*, vol. 8, no. 1, pp. 1–8, Dec. 2018.

[148] C. Gerlein-Safdi and C. S. Ruf, "A CYGNSS-based algorithm for the detection of inland waterbodies," *Geophys. Res. Lett.*, vol. 46, no. 21, pp. 12065–12072, Nov. 2019.

[149] M. Morris, C. Chew, J. T. Reager, R. Shah, and C. Zuffada, "A novel approach to monitoring wetland dynamics using CYGNSS: Everglades case study," *Remote Sens. Environ.*, vol. 233, Nov. 2019, Art. no. 111417.

[150] M. M. Al-Khaldi, J. T. Johnson, S. Gleason, C. C. Chew, C. Gerlein-Safdi, R. Shah, and C. Zuffada, "Inland water body mapping using CYGNSS coherence detection," *IEEE Trans. Geosci. Remote Sens.*, early access, Jan. 18, 2021, doi: 10.1109/TGRS.2020.3047075.

[151] M. Wiehl, B. Legrésy, and R. Dietrich, "Potential of reflected GNSS signals for ice sheet remote sensing," *Prog. Electromagn. Res.*, vol. 40, pp. 177–205, Jan. 2003.

[152] K. M. Larson, E. D. Gutmann, V. U. Zavorotny, J. J. Braun, M. W. Williams, and F. G. Nievinski, "Can we measure snow depth with GPS receivers?" *Geophys. Res. Lett.*, vol. 36, no. 17, 2009, Art. no. L17502.

[153] M. D. Jacobson, "Inferring snow water equivalent for a snow-covered ground reflector using GPS multipath signals," *Remote Sens.*, vol. 2, no. 10, pp. 2426–2441, Oct. 2010.

[154] N. Rodriguez-Alvarez, A. Aguasca, E. Valencia, X. Bosch-Lluis, A. Camps, I. Ramos-Perez, H. Park, and M. Vall-Llossera, "Snow thickness monitoring using GNSS measurements," *IEEE Geosci. Remote Sens. Lett.*, vol. 9, no. 6, pp. 1109–1113, Nov. 2012.

[155] A. M. Semmling, G. Beyerle, R. Stosius, G. Dick, J. Wickert, F. Fabra, E. Cardellach, S. Ribó, A. Rius, A. Helm, S. B. Yudanov, and S. d'Addio, "Detection of arctic ocean tides using interferometric GNSS-R signals," *Geophys. Res. Lett.*, vol. 38, no. 4, Feb. 2011, Art. no. L04103.

[156] F. Fabra, "GNSS-R as a source of opportunity for remote sensing of the cryosphere," Ph.D. dissertation, Univ. Politecnica Catalunya, Barcelona, Spain, 2013. Accessed: May 10, 2020. [Online]. Available: https://www.tesisenred.net/handle/10803/117605

[157] F. Fabra, E. Cardellach, A. Rius, S. Ribo, S. Oliveras, O. Nogues-Correig, M. B. Rivas, M. Semmling, and S. D'Addio, "Phase altimetry with dual polarization GNSS-R over sea ice," *IEEE Trans. Geosci. Remote Sens.*, vol. 50, no. 6, pp. 2112–2121, Jun. 2012.

[158] A. Komjathy, J. Maslanik, V. U. Zavorotny, P. Axelrad, and S. J. Katzberg, "Sea ice remote sensing using surface reflected GPS signals," in *Proc. IEEE IGARSS*, Honolulu, HI, USA, Jul. 2000, pp. 2855–2857.

[159] S. Gleason, "Towards sea ice remote sensing with space detected GPS signals: Demonstration of technical feasibility and initial consistency check using low resolution sea ice information," *Remote Sens.*, vol. 2, no. 8, pp. 2017–2039, Aug. 2010.

[160] E. Cardellach, F. Fabra, O. Nogués-Correig, S. Oliveras, S. Ribó, and A. Rius, "GNSS-R ground-based and airborne campaigns for ocean, land, ice, and snow techniques: Application to the GOLD-RTR data sets: GNSS-R CAMPAIGNS," *Radio Sci.*, vol. 46, no. 6, pp. 1–16, Dec. 2011.

[161] V. Zavorotny and C. Zuffada, "A novel technique for characterizing the thickness of first-year sea-ice with the GPS reflected signal," *EOS Trans. AGU*, vol. 83, no. 47, p. 0980, 2002.

[162] M. Belmonte, "Bistatic scattering of global positioning system signals from arctic sea ice," Ph.D. dissertation, Univ. Colorado, Boulder, CO, USA, 2007.

[163] M. B. Rivas, J. A. Maslanik, and P. Axelrad, "Bistatic scattering of GPS signals off arctic sea ice," *IEEE Trans. Geosci. Remote Sens.*, vol. 48, no. 3, pp. 1548–1553, Mar. 2010.

[164] H. Carreno-Luengo, S. Lowe, C. Zuffada, S. Esterhuizen, and S. Oveisgharan, "Advancing GNSS-R ocean scatterometry and altimetry; SMAP + CYGNSS," in *Proc. IEEE GRSS Spec. Meeting Reflectometry Using GNSS Other Signals Opportunity*, Ann Arbor, MI, USA, May 2017. Accessed: May 10, 2020. [Online]. Available: http://www.gnssr2017.org/images/Wednesday_morning/GNSS+R2017_WE_AM_2_Carreno-Luengo_SMAP_Scatterometry.pdf

[165] H. Carreno-Luengo, S. T. Lowe, C. Zuffada, S. Esterhuizen, and S. Oveisgharan, "GNSS-R from the SMAP and CyGNSS missions: Application to polarimetric scatterometry and ocean altimetry," in *Proc. IEEE IGARSS*, Fort Worth, TX, USA, Jul. 2017, pp. 5019–5021.

[166] A. Alonso-Arroyo, V. U. Zavorotny, and A. Camps, "Sea ice detection using U.K. TDS-1 GNSS-R data," *IEEE Trans. Geosci. Remote Sens.*, vol. 55, no. 9, pp. 4989–5001, Sep. 2017.

[167] Q. Yan and W. Huang, "Sea ice sensing from GNSS-R data using convolutional neural networks," *IEEE Geosci. Remote Sens. Lett.*, vol. 15, no. 10, pp. 1510–1514, Oct. 2018.

[168] Q. Yan and W. Huang, "Detecting sea ice from TechDemoSat-1 data using support vector machines with feature selection," *IEEE J. Sel. Topics Appl. Earth Observ. Remote Sens.*, vol. 12, no. 5, pp. 1409–1416, May 2019.

[169] B. J. Southwell and A. G. Dempster, "Sea ice transition detection using incoherent integration and deconvolution," *IEEE J. Sel. Topics Appl. Earth Observ. Remote Sens.*, vol. 13, pp. 14–20, 2020.
[170] Q. Yan and W. Huang, "Sea ice thickness measurement using spaceborne GNSS-R: First results with TechDemoSat-1 data," *IEEE J. Sel. Topics Appl. Earth Observ. Remote Sens.*, vol. 13, pp. 577–587, 2020.
[171] Y. Zhu, T. Tao, J. Zou, K. Yu, J. Wickert, and M. Semmling, "Spaceborne GNSS reflectometry for retrieving sea ice concentration using TDS-1 data," *IEEE Geosci. Remote Sens. Lett.*, vol. 18, no. 4, pp. 612–616, Apr. 2021.
[172] N. Rodriguez-Alvarez, B. Holt, S. Jaruwatanadilok, E. Podest, and K. C. Cavanaugh, "An arctic sea ice multi-step classification based on GNSS-R data from the TDS-1 mission," *Remote Sens. Environ.*, vol. 230, Sep. 2019, Art. no. 111202.
[173] A. Rius, E. Cardellach, F. Fabra, W. Li, S. Ribó, and M. Hernández-Pajares, "Feasibility of GNSS-R ice sheet altimetry in greenland using TDS-1," *Remote Sens.*, vol. 9, no. 7, p. 742, Jul. 2017.
[174] W. Li, E. Cardellach, F. Fabra, S. Ribó, and A. Rius, "Measuring greenland ice sheet melt using spaceborne GNSS reflectometry from TechDemoSat-1," *Geophys. Res. Lett.*, vol. 47, no. 2, pp. 1–10, Jan. 2020.

HUGO CARRENO-LUENGO (Senior Member, IEEE) received the Ingeniero Aeronautico degree (Plan Antiguo de Estudios, "bachelor+master"), specialization in spacecrafts, from the Escuela Técnica Superior de Ingenieros Aeronáuticos (ETSIA), Universidad Politécnica de Madrid (UPM), Madrid, Spain, in 2010, and the Ph.D. degree *(cum laude)* from the Department of Signal Theory and Communications (TSC), Universitat Politécnica de Catalunya (UPC), Barcelona, Spain, in 2016.

From 2009 to 2010, he performed the final degree project with the Department of Aircrafts and Space Vehicles, UPM. In 2011, he performed the Master of Space Science and Technology at UPC. From 2011 to 2016, he was involved in the design and development of the first-ever Nano-Satellite for Earth Remote Sensing using GNSS-R with the Institut d'Estudis Espacials de Catalunya (IEEC). From 2012 to 2015, he was a Principal Investigator (PI) of the TORMES and TORMES 2.0 projects within ESA's REXUS/BEXUS and a Co-PI of the E-GEM FP7 Project. From 2013 to 2014, he was a Visiting Researcher with ESA-ESTEC, DLR, Esrange Space Center. In Summer 2016, he was invited by the China Great Wall Industry Corporation (CGWIC) to assist the launch campaign of the 3Cat-2 CubeSat at Jiuquan Satellite Launch Center. He was holding a postdoctoral position at the NASA Jet Propulsion Laboratory (JPL), Pasadena, CA, USA, from 2016 to 2017, working in a GNSS-Reflectometry experiment within NASA's Soil Moisture Active Passive (SMAP) mission. This work set the basis for the development of the new SMAP operational mode. From 2017 to 2019, he was holding a postdoctoral position at CTTC with the first position of the "Juan de la Cierva" postdoctoral research program, by the Ministerio de Ciencia e Innovacion. He worked on the development of methodologies for a synergistic use of GNSS-R and microwave radiometry towards a "federated" operation of NASA's CYclone Global Navigation Satellite System (CYGNSS) and SMAP missions. During these years, he was a Research Affiliate within NASA's Extended CYGNSS Science Team. Since 2019, he has been a NASA Science Mission Directorate/CLaSP-UMich Research Scientist working directly with the PI of NASA's CYGNSS mission. He is developing the updated CYGNSS end-to-end simulator and working in new freeze/thaw (F/T) retrieval algorithms. He has participated in ten international research projects (NASA, ESA, and FP7), being PI in three and co-PI in one of them. He has participated in three national research projects (MINECO), being PI of two of them. Additionally, he has participated in technology transfer activities at CTTC and within the Sesar project (European Union). He has reviewed the book *Climate Change and Extreme Events: Do We Know Enough?* (Elsevier). He has published 20 journal articles (15 as first author) in international peer-reviewed journals (Q1) and 47 international conference proceedings, including IGARSS papers (37 as first author). His research interests include the use of GNSS-Reflectometry techniques for Earth remote sensing over land surfaces from small satellites. His research work has attracted 545 citations up to now in this small community, reporting an H-index of 14 and i-10 index of 17.

Dr. Carreno-Luengo is a member of the IEEE GRSS and the IEEE GRSS Technical Committee on Standards for Earth Observations. He was a recipient of two IEEE and one NASA student travel grants, from 2012 to 2015, the IEEE GRSS Award for the Best Ph.D. Thesis in Geoscience and Remote Sensing, the Serra Hunter Programme, the CAS's President's International Fellowship Initiative (PIFI), in 2017, the UPC Special Award in Science, in 2018, and the MDPI Remote Sensing Postdoctoral Award, in 2019. He has advised 13 final degree and two master thesis. He was a recipient of the Ph.D. Fellowship by the IEEC. He was the Session Chair at the 2015, 2017, 2018, and 2019 IEEE International Geoscience and Remote Sensing Symposium (IGARSS), and the 2020 NASA CYGNSS Science Team Meeting. He is serving as the Chair for the IEEE GRSS Working Group P4003 (Standard for Global Navigation Satellite System-Reflectometry Data and Metadata Content). He has managed several students teams within ESA REXUS/BEXUS (ESA Educational Office). He is a Topic Editor and a member of the Reviewer Board of *Remote Sensing* (MDPI). He is a Guest Editor of the *Remote Sensing* (MDPI) Special Issue on Advanced RF Sensors and Remote Sensing Instruments and Special Issue on GNSS-R Earth Remote Sensing from SmallSats. He is an Associate Editor of *Earth* (MDPI). He has reviewed 63 articles in high impact factor journals, such as IEEE Transactions on Geoscience and Remote Sensing (TGRS), IEEE Journal of Selected Topics in Applied Earth Observations and Remote Sensing (JSTARS), IEEE Geoscience and Remote Sensing Letters (GRSL), *Remote Sensing and Sensors* (MDPI), *Advances in Space Research* (Elsevier), and *Radio Science* (AGU). He served on the panel review for the NASA's Research Opportunities in Space and Earth Science (ROSES) GNSS Program, in 2020 (24 proposals). He has been serving as an External Reviewer (panelist) for the European Commission and other public research and development centers from EU members. He has provided 51 talks to international research societies, including 11 invited presentations (IGARSS and ESA ARSI+KEO). Some of his results have been included in the cover page of the *IEEE Geoscience and Remote Sensing Magazine*, in December 2014, and the IEEE Journal of Selected Topics in Applied Earth Observations and Remote Sensing (JSTARS) Special Issue on CYGNSS Early on Orbit Performance, in January 2019. Additionally, he has the qualification of an Assistant Professor by the Spanish National Agency for Quality Assessment and Accreditation and of a Tenure Track Lecturer by the Catalan University Quality Assurance Agency. He held a total of 42 honors and awards. He has actively participated in numerous outreach activities (national and international).

ADRIANO CAMPS (Fellow, IEEE) was born in Barcelona, Spain, in 1969. He received the degree in telecommunications engineering and the Ph.D. degree in telecommunications engineering from the Universitat Politècnica de Catalunya (UPC), Barcelona, Spain, in 1992 and 1996, respectively.

From 1991 to 1992, he was as an Erasmus Fellowship at the ENS des Télécommunications de Bretagne, France. Since 1993, he has been with the Electromagnetics and Photonics Engineering Group, Department of Signal Theory and Communications, UPC, where he was an Assistant Professor, an Associate Professor, in 1997, and has been a Full Professor, since 2007. In 1999, he was on sabbatical leave with the Microwave Remote Sensing Laboratory, University of Massachusetts. Since 1993, he has been deeply involved with the European Space Agency SMOS Earth Explorer Mission, from the instrument and algorithmic points of view, performing field experiments. Since 2001, he has been studying the use of GNSS-R techniques to perform the sea-state correction needed to retrieve salinity from L-band radiometric observations. His research interests are focused in microwave remote sensing, with special emphasis in microwave radiometry by aperture synthesis techniques and remote sensing using signals of opportunity (GNSS-R). He has published over 203 articles in peer-reviewed journals, six book chapters, one book, and more than 425 international conference presentations, holds 12 patents, and has advised 23 Ph.D. Thesis students (more than eight on-going), and more than 120 final projects, and M.Eng. Thesis. According to Publish or Perish (Google Scholar) his publications have received more than 6347/9547 citations and his H-Index is 38/47 according to Scopus/Google Scholar. He is currently the Scientific Coordinator of the CommSensLab "María de Maeztu" Excellence Research Unit, where he co-led the Remote Sensing Laboratory and co-leads the UPC

NanoSat Laboratory. He is the PI of the first four UPC nanosatellites: 3Cat-1 and a 1U CubeSat with seven small technology demonstrators and scientific payloads, 3Cat-2, a 6U CubeSat with the first dual-frequency dual-polarization GNSS-R payload, launched on August 15, 2016, using a Chinese LM-D2 rocket, 3Cat-4, a 1U Cubesat with a software defined radio to implement a microwave radiometer, a GNSS-Reflectomer, and an AIS receiver, and FSSCAT, a tandem mission formed by two 6U CubeSats, overall winner of the Copernicus masters competition 2017. He has been a member of the IGARSS Technical Program Committee, since 2002. He was the Chair of uCal 2001, the IGARSS 2007 Technical Program Committee Co-Chair, the Co-Chair of GNSS-R'10, and the Co-Chair of IGARSS 2020 and the 6th FFSS Workshop. He was an Associate Editor of *Radio Science*, IEEE Geoscience and Remote Sensing Letters. He is currently an Associate Editor of the IEEE Transactions on Geoscience and Remote Sensing. He was the President-Founder of the IEEE Geoscience and Remote Sensing Society (GRSS) Chapter, Spain. He has been a member of the IEEE Geoscience and Remote Sensing Society Administrative Committee, since 2002, where he has been the Newsletter Editor, the Web Editor, the Vice President of Information Resources, the Vice President of Meetings and Symposia, the Executive Vice President, and the President of the IEEE Geoscience and Remote Sensing Society, in 2017 and 2018. In 1993, he was a recipient of the Second National Award of University Studies, the INDRA Award of the Spanish Association of Telecommunication Engineers to the Best Ph.D. in Remote Sensing, in 1997; the Extraordinary Ph.D. Award at the Universitat Politècnica de Catalunya, in 1999; the Research Distinction of the Generalitat de Catalunya for Contributions to Microwave Passive Remote Sensing, in 2002; the European Young Investigator Award, in 2004; and the ICREA Academia Award, in 2009 and 2015. In 2011, he was elevated to the grade of fellow of the Institute of Electrical and Electronic Engineers for "For contributions to microwave remote sensing of land and sea surfaces." Finally, as a member of the Microwave Radiometry Group, UPC, he received the 1st Duran Farell and the Ciutat de Barcelona awards for Technology Transfer, in 2000, 2001, and 2004, and the "Salvái Campillo" Award of the Professional Association of Telecommunication Engineers of Catalonia for the most innovative research project for MIRAS/SMOS related activities, and the 7th Duran Farell Award for Technological Research for the work on GNSS-R instrumentation and applications, in 2010. In 2015, he and Mr. Querol was also a recipient of the European Satellite Navigation Competition Award-Barcelona Challenge for the FENIX system to detect and mitigate radio frequency interference in satellite navigation receivers, and in 2017, he was the Winner of the Copernicus Masters ESA Sentinel Small Satellite Challenge and the Overall Winner of 2017 Copernicus Masters Competition.

CHRIS RUF (Fellow, IEEE) received the B.A. degree in physics from the Reed College, Portland, OR, USA, in 1982, and the Ph.D. degree in electrical and computer engineering from the University of Massachusetts at Amherst, Amherst, MA, USA, in 1987.

He is currently a Frederick Bartman Collegiate Professor of climate and space science with the University of Michigan, Ann Arbor, MI, USA, and a Principal Investigator of the Cyclone Global Navigation Satellite System (GNSS) NASA Earth Venture Mission. He was with Intel Corporation, Hughes Space and Communication, the NASA Jet Propulsion Laboratory, and Penn State University. His research interests include GNSS-R remote sensing, microwave radiometry, atmosphere and ocean geophysical retrieval algorithm development, and sensor technology development.

Dr. Ruf is a member of the American Geophysical Union, the American Meteorological Society, and the Commission F of the Union Radio Scientifique Internationale. He is the former Editor-in-Chief of the IEEE Transactions on Geoscience and Remote Sensing. He was on the editorial boards of *Radio Science* and the *Journal of Atmospheric and Oceanic Technology*. He was a recipient of four NASA Certificates of Recognition and seven NASA Group Achievement Awards, the 1997 TGRS Best Paper Award, the 1999 IEEE Resnik Technical Field Award, the 2006 IGARSS Best Paper Award, and the 2014 IEEE GRSS Outstanding Service Award.

NICOLAS FLOURY received the M.Sc. degree in engineering from Telecom ParisTech, Paris, France, in 1993, and the Ph.D. degree in applied physics from Paris Diderot University, Paris, in 1999. Since then, he has been with the European Space Research and Technology Centre, European Space Agency, Noordwijk, The Netherlands, where he is currently the Head of the Wave Interaction and Propagation Section. His research interests include signal processing and electromagnetic modeling applied to microwave interaction with natural media.

MANUEL MARTIN-NEIRA (Senior Member, IEEE) received the M.S. and Ph.D. degrees in telecommunication engineering from the School of Telecommunication Engineering, Polytechnic University of Catalonia, Spain, in 1986 and 1996, respectively.

From 1989 to 1992, he joined GMV, a Spanish firm, where he was responsible for several projects of the European Space Agency (ESA) related to GPS spacecraft navigation with applications to precise landing and attitude determination. Since 1992, he has been the in-charge of the radiometer activities within the Payload, Equipment, and Technology Section, ESA. During this period, he has developed new concepts for constellations of small satellites for Earth observation. In particular, he holds a patent on the PARIS concept for the use of GNSS signals reflected from the ocean.

Dr. Martin-Neira has been a member of the Academie des Technologies of France, since 2009. He received the Confirmed Inventor Award from the Director of ESA, in 2002. He is currently the Instrument Principal Engineer of ESA's Soil Moisture and Ocean Salinity Earth Explorer Opportunity Mission. He received a fellowship to work on radiometry at the European Space Research and Technology Center, Noordwijk, The Netherlands, in 1988.

TIANLIN WANG (Member, IEEE) received the B.E. degree in electrical engineering from the East China University of Science and Technology, Shanghai, China, the M.S. degree in radio physics from Fudan University, Shanghai, and the M.S. and Ph.D. degrees in electrical engineering from the University of Michigan, Ann Arbor, MI, USA.

His research work contributed to calibration/validation and geophysical retrieval for the Cyclone Global Navigation Satellite System NASA Earth Venture mission. His research interests include microwave remote sensing, microwave measurements, and radio frequency (RF) circuits. He is a member of Tau Beta Pi, the Eta Kappa Nu, the American Geophysical Union (AGU), and the Institute of Navigation (ION). He is an Early Career Member of the Commission F of the U.S. National Committee (USNC) for the Union Radio Scientifique Internationale (URSI). He was a recipient of the 2018 IEEE Mikio Takagi Student Prize, the Outstanding Student Presentation Award at 2018 AGU Fall Meeting, the 2020 Richard F. and Eleanor A. Towner Prize for Distinguished Academic Achievement and Distinguished Leadership Award from the University of Michigan, and the 2021 Ernest K. Smith USNC-URSI Student Prize (2nd Place).

SIRI JODHA KHALSA (Senior Member, IEEE) received the B.A. degree in physics from the University of California at Irvine, Irvine, and the Ph.D. degree in atmospheric sciences from the University of Washington, Seattle. Since 1993, he has been supporting NASA's Distributed Active Archive Center (DAAC) at the National Snow and Ice Data Center (NSIDC), where he performs science evaluation and algorithm support for data products coming from NASA's Earth observing satellites, leading informatics, and cryospheric research projects. He has published in the fields of satellite remote sensing, glaciology, global atmospheric teleconnections, air-sea interaction, boundary layer turbulence, and Earth science informatics. He is currently the Chair of the Institute of Electrical and Electronics Engineers (IEEE) Geoscience and Remote Sensing Society (GRSS) Standards Committee and the IEEE Oceanic Engineering Society's Technical Committee on Ocean Observation and Environmental Sustainability.

MARIA PAOLA CLARIZIA (Senior Member, IEEE) received the master's degree in telecommunications engineering from the University of Sannio, Benevento, Italy, in 2007, and the Ph.D. degree in ocean remote sensing using GNSS-R from the University of Southampton, Southampton, U.K., in 2012.

She has more than ten years of experience in remote sensing, with a focus on GNSS-Reflectometry, working in academia and private industry. She was a Research Engineer with Starlab, Barcelona, Spain. She was a Research Scientist with the National Oceanography Centre, Southampton, U.K. She was a Postdoctoral Research Fellow with the University of Michigan, Ann Arbor, MI, USA, and the University of Southampton, U.K., working on the CYGNSS mission for ocean and land applications. She is currently a GNSS-R Technical Manager with Deimos Space, Harwell Oxford, U.K., and a member of the CYGNSS Science Team. Her research interests include GNSS-reflectometry, altimetry and scatterometry, electromagnetic scattering models, retrieval algorithms, data analysis, and statistical processing.

JENNIFER REYNOLDS received the bachelor's degree in environmental science from the University of Exeter, Exeter, U.K., in 2017, and the master's degree in space and exploration systems from the University of Leicester, Leicester, U.K., in 2018. Her bachelor's thesis was on using machine learning techniques to estimate the number of dust devil tracks in the Argyre and Hellas Planitia regions of Mars. Since 2018, she has been a Global Navigation Satellite System (GNSS) Reflectometry Engineer at Deimos Space, Harwell Oxford, U.K. Her works include GNSS-reflectometry, retrieval algorithms, data analysis, and machine learning.

JOEL JOHNSON received the bachelor's degree in electrical engineering from the Georgia Institute of Technology, in 1991, and the S.M. and Ph.D. degrees from the Massachusetts Institute of Technology, in 1993 and 1996, respectively. He is currently the Burn and Sue Lin Professor with the Department of Electrical and Computer Engineering and the ElectroScience Laboratory, The Ohio State University. His research interests include microwave remote sensing, propagation, and electromagnetic wave theory. He is a member of commissions B and F of the International Union of Radio Science (URSI), Tau Beta Pi, Eta Kappa Nu, and Phi Kappa Phi. He received the 1993 Best Paper Award from the IEEE Geoscience and Remote Sensing Society, the National Science Foundation CAREER Award, and the PECASE Award Recipient, in 1997. He was named an Office of Naval Research Young Investigator. He was recognized by the U.S. National Committee of URSI, as a Booker Fellow, in 2002.

ANDREW O'BRIEN (Member, IEEE) received the Ph.D. degree in electrical engineering from The Ohio State University, Columbus, OH, USA, in 2009. From 2005 to 2009, he was a Graduate Research Associate with the ElectroScience Laboratory, The Ohio State University. He worked in the area of adaptive global navigation satellite system (GNSS) antenna arrays and precise GNSS receivers on complex platforms. He is currently a Research Scientist with the ElectroScience Laboratory, The Ohio State University. His primary research interests include spaceborne GNSS remote sensing using cyclone global navigation satellite system (CYGNSS), TDS-1, and soil moisture active passive (SMAP). His other research activities include GNSS antenna arrays, adaptive antenna electronics, airborne geolocation, and radar systems. He is a member of the CYGNSS Science Team and has supported the development of end-to-end simulations and engineering activities.

CARMELA GALDI (Member, IEEE) received the Dr.Eng. and Ph.D. degrees in electronic engineering from the Università degli Studi di Napoli Federico II, Naples, Italy, in 1992 and 1997, respectively. In 1995, she was an Erasmus Fellowship with the Signal Processing Division, University of Strathclyde, Glasgow, U.K. In 1997, she was a Visiting Scientist with the University College London, London, U.K., and working on statistical models of radar backscattering from natural surfaces with the Defense Evaluation and Research Agency, Malvern, U.K. From 1997 to 2000, she was Postdoctoral Researcher with the Università degli Studi di Napoli Federico II. In 2000, she joined the Università degli Studi del Sannio, Benevento, Italy, where she is currently an Associate Professor in telecommunications. Her research interests include statistical signal processing, non-Gaussian models of radar backscattering, and global navigation satellite system reflectometry. She was with the Organizing Committee of the IEEE 2008 Radar Conference. She was the Co-Chair of the IEEE GNSS+R 2019 Specialist Meeting. She has cooperated with the National Oceanography Centre (NOC), Southampton, U.K., on a project about GNSS-R of the ocean surface. She is currently associated with the NASA CYGNSS Project, as an External Science Team Member, working on the development of science algorithms for GNSS reflectometry.

MAURIZIO DI BISCEGLIE (Member, IEEE) was born in Naples, Italy. He received the Ph.D. degree in electronic and communications engineering from the Università degli Studi di Napoli Federico II, Naples, Italy, in 1993. Since 1998, he has been with the Università degli Studi del Sannio, Benevento, Italy, as an Associate Professor of telecommunications. He was a Visiting Scientist with the University College of London, London, U.K., and the Defense Evaluation and Research Agency, Malvern, U.K. His research interests include statistical signal processing with applications to stochastic modeling and GNSS reflectometry. He was with the Organizing Committee of the Italian Phase of European AQUA Thermodynamic Experiment Mission, in 2004, the Co-Chair of the NASA Direct Readout Conference, in 2005, and the Organizing Committee of the IEEE 2008 Radar Conference. Since 2016, he has been a member of the NASA CYGNSS External Science Team.

ANDREAS DIELACHER received the M.Sc. degree in computer engineering from Technical University of Vienna, Austria, in 2010. He is currently pursuing the Ph.D. degree with the Austrian CubeSat Project Passive REflectomeTer and DosimeTrY, RUAG Space GmbH, Vienna, where he is assigned as a Project Engineer for the passive reflectometer payload. He is with the Projects Engineering Group, RUAG Space GmbH. He was involved in various designs, including a GPS L2C receiver, and he has led the passive reflectometry projects, namely, PARIS Correlator, GEROS-ISS, and the PACO for CubeSat study at RUAG Space GmbH.

PHILIP JALES received the M.Phys. degree in physics from The University of Manchester, Manchester, U.K., in 2007, and the Ph.D. degree in GNSS reflectometry techniques from the University of Surrey, Guildford, U.K., in 2012, with a focus on new receiver approaches. He is currently a Senior Engineer with Surrey Satellite Technology Ltd. (SSTL), Surrey, U.K., working on the reflectometry-capable space global navigation satellite system receivers, the SGRReSI and SGR-Axio. He is supporting the NASA CYGNSS mission and the TechDemoSat-1 reflectometry exploitation experiment.

MARTIN UNWIN is currently pursuing the Ph.D. degree in spaceborne GPS with the University of Surrey, Guildford, U.K.

He initiated and led the GPS Team, Surrey Satellite Technology Ltd. (SSTL), Surrey, U.K., designing the SGR-20 space GPS receiver which flew on UoSAT-12 and Proba-1. The GPS team succeeded in demonstrating autonomous orbit control, attitude determination in orbit, operation of GPS above the GPS constellation, and the feasibility of GPS reflectometry on the U.K. disaster monitoring constellation satellite. He had involvement in GIOVE-A and Galileo FOC projects from the beginning. He is currently a Principal Engineer with SSTL and working on the development of the SGR-Axio receiver, the SGR-ReSI exploitation on TechDemoSat-1, and the NASA CYGNSS mission. He received the Institute of Navigation Tycho Brahe Award 2011 and the GPS World Leadership Award, in 2012.

LUCINDA KING (Graduate Student Member, IEEE) received the bachelor's degree in experimental and theoretical physics from the University of Cambridge, Cambridge, U.K., in 2013. She is currently pursuing the Ph.D. degree in electrical and electronic engineering with the University of Surrey, Guildford, U.K., where her research focuses on the use of global navigation satellite system (GNSS) reflectometry for monitoring land parameters and the use of new GNSS signals. From 2015 to 2018, she worked as a Space Systems Engineer with Airbus Defence and Space, on a variety of projects related to GNSS, including the Galileo ground control segment, software receiver development, and research and development.

GIUSEPPE FOTI received the M.Eng. degree in electronics engineering from the University of Catania, Catania, Italy, in 2000, and the M.Sc. degree in oceanography from the University of Southampton, Southampton, U.K., in 2013. In 2001, he joined the Communication Systems Section, European Space Agency, Noordwijk, The Netherlands, where he conducted research in the field of spread-spectrum techniques for packet access in broadband satellite systems. From 2003 to 2010, he served as a Patent Examiner in the Principal Directorate of telecommunications with the European Patent Office, Rijswijk, The Netherlands. In 2013, he joined the Satellite Oceanography Section, National Oceanography Centre, Southampton, where he currently works as a Research Scientist. His current research interest includes remote sensing of the oceans, with special emphasis on techniques using signals of opportunity.

RASHMI SHAH (Senior Member, IEEE) received the M.S. degree in engineering and the Ph.D. degree in aeronautics and astronautics from Purdue University, West Lafayette, IN, USA, in 2010 and 2014, respectively. Her research was on remote sensing using digital communication signals of opportunity. Since 2014, she has been a Research Technologist with the NASA Jet Propulsion Laboratory, Pasadena, CA, USA, where she is leading signals of opportunity effort. Her research interest includes the use of satellite digital communication signals as a source of opportunity for remote sensing applications.

DANIEL PASCUAL (Member, IEEE) was born in Barcelona, Spain, in 1985. He received the B.Sc. and plus five degree in telecommunications engineering, with a focus on communications, and the M.Sc. and plus two degree in research on information and communication technologies from the Universitat Politècnica de Catalunya (UPC), Barcelona, Spain, in 2011 and 2014, respectively, where he is currently pursuing the Ph.D. degree in GNSS reflectometry (GNSS-R) with the Passive Remote Sensing Group, focused on GNSS-R real-time data processing using FPGA.

BILL SCHREINER, photograph and biography not available at the time of publication.

MILAD ASGARIMEHR received the M.Sc. degree in geodesy from the K. N. Toosi University of Technology, Tehran, Iran, in 2015. He is currently pursuing the Ph.D. degree with the GFZ German Research Centre for Geosciences, Potsdam, Germany, and Technische Universität Berlin, Berlin, Germany. His master's thesis was on constellation design of positioning systems and LEO global navigation satellite system (GNSS) remote sensing satellites using evolutionary techniques. He started his scientific contribution authoring two ISI listed peer-reviewed articles, as a master student. After being involved in GNSS precise positioning and deformation analyses of important structures, as a Geodetic Engineer, he joined the GFZ German Research Centre for Geosciences and the Technische Universität Berlin, in 2017, for doctoral research. He was awarded the Young Academy Fellowship by Geo.X, the Geoscientific network in Berlin and Potsdam area, as an Interdisciplinary Young Researcher in Geo Data Science in cooperation with the University of Potsdam, Potsdam. His Ph.D. dissertation is dedicated to the space-borne GNSS reflectometry concept as an ocean scatterometry technique and remote sensing using signals of opportunity. His research interests include developing innovative approaches and applications in GNSS remote sensing taking the advantages of the methodological field of data science.

JENS WICKERT received the Graduate degree in physics from the Technical University of Dresden, Dresden, Germany, in 1989, and the Ph.D. degree in geophysics/meteorology from the Karl-Franzens-Universität Graz, Graz, Austria, in 2002. He was with several German geoscience research institutes. He currently holds a joint professorship at the GFZ German Research Centre for Geosciences, Potsdam, Germany, and with the Technical University of Berlin, Berlin, Germany, on global navigation satellite system (GNSS) remote sensing, navigation, and positioning. He is the Deputy GFZ Section Head Space Geodetic Techniques and the GFZ Speaker of the Atmosphere and Climate Research Program of the German Helmholtz Association. He has authored or coauthored more than 250 ISI listed publications on GNSS Earth observation and is coordinating numerous research projects in this research field. He was a Principal Investigator of the pioneering GPS radio occultation experiment aboard the German CHAMP satellite and was coordinating the GEROS-ISS proposal to the European Space Agency. He is the Chair and Co-Chair of the Science Advisory Group of the GEROS-ISS and G-TERN missions, respectively.

SERNI RIBO (Member, IEEE) received the M.S. degree in telecommunications engineering and the Ph.D. degree from the Polytechnic University of Catalonia, Barcelona, Spain, in 1999 and 2005, respectively. In 2000, he joined the European Space Agency (ESA), Noordwijk, The Netherlands, with a grant from the Spanish Ministry of Science and Technology, where he was involved in synthetic aperture radiometry technology. Since 2003, he has been with the Institute of Space Sciences (ICE), Spanish National Research Council (CSIC), Institut d'Estudis Espacials de Catalunya (IEEC), Barcelona. He is currently involved in the development of new ocean altimetry and scatterometry global navigation satellite system (GNSS) reflection instrumentation.

ESTEL CARDELLACH (Senior Member, IEEE) received the Ph.D. degree in physics from the Polytechnic University of Catalonia, Barcelona, Spain, in 2002. She has been involved in scientific applications of global navigation satellite systems (GNSSs) for remote sensing of the Earth, such as extraction of geophysical information of the GNSS reflected signals, radio occultation, and geodetic techniques. From 2002 to 2003, she was a National Research Council Awardee for a postdoctoral position at the NASA Jet Propulsion Laboratory, Pasadena, CA, USA. From 2003 to 2005, she was a Postdoctoral Researcher with the Harvard Smithsonian Center for Astrophysics, Cambridge, MA, USA. Since 2005, she has been with the Institute of Space Sciences (ICE), Spanish National Research Council (CSIC), Institut d'Estudis Espacials de Catalunya (IEEC), Barcelona. She is a Principal Investigator of the space-borne experiment Radio-Occultation and Heavy Precipitation aboard the PAZ Low Earth Orbiter funded by Spanish grants.